Chapter 5

Annealing parameter optimization and TSL/OSL characteristics

5.1 Introduction

TL/OSL phosphor is a material that exhibits the phenomenon of luminescence due to thermal/optical stimulation after it has been exposed to ionizing radiations. Many different types of phosphors are used in the various TL/OSL applications like radiation dosimetry in nuclear plants, medical dosimetry, environmental dosimetry and space research. Use of nano-phosphors for TL/OSL applications is an active field of research and it holds many possibilities which have to be explored.

The TL/OSL characteristics of the synthesised nano CaF_2 are examined in this chapter. The 'as prepared' phosphor did not give any TL response. In order to make it TL sensitive annealing treatment was needed. The study undertaken to find the best annealing parameter for optimal TL response furthers our knowledge as to the TL behavior of the phosphor with respect to the annealing treatment received by it.

The chapter describes how the various TL parameters are derived using different methods. The dose response and linearity of dose response is also reported along with the effect of heating rate on the glow curve. The behavior of the phosphor under UV and blue light stimulation is investigated. The emission is studied using different filter combinations to get insight into the spectral characteristics of the emission. The correlation between the TL causing traps and the OSL causing traps is investigated. The Radio-Luminescence (RL) response of phosphor is also presented.

5.2 Annealing

The effect of annealing on the TL properties of different phosphors has been well reported. It has been established that annealing is an essential requirement for both natural and synthetic

TL/OSL phosphors. Annealing is a thermal treatment process where the samples are heated up to a specific temperature, kept at this temperature for a specific duration of time, and then cooled down to room temperature. The annealing parameters like annealing temperature, annealing duration and annealing atmosphere critically affect the luminescent behavior of the phosphor. Thus it is important to maintain consistency in these parameters [1]. After annealing the phosphor is no longer of nano size.

The 'as synthesised' CaF_2 was non-luminescent. However, after annealing it exhibited TL. Though its annealing parameters are given in literature [2-7], there is no definite agreement among them on this subject. El-Kolaly *et al* [2] reports the increase in sensitivity in natural CaF_2 as annealing temperatures are increased till 850 ˚C and then it decreases with further increase in temperature. When annealed in air, the sensitivity decreases with increase in annealing temperature. At 850˚C, it approaches zero sensitivity—it is at this same point where the sensitivity trend reverses for vacuum annealing. Their duration of annealing was 1 hour. C. M. Sunta reports that natural CaF_2 has to be annealed first at 400 ˚C in air for an hour to remove organic impurity. Then it should be heated at 700 ˚C in oxygen free, nitrogen atmosphere to anneal out the high temperature natural TL—otherwise the phosphor becomes sensitive to light (photo-transfer) [3-4]. In a later paper [5] which came after 10 years, the same author reports annealing at 600 ˚C for 30 min and at 400 ˚C for 30 min and compares the result. 400 ˚C for 30 min gave better result. Due to all this disagreement in the literature, the best annealing parameters for the prepared CaF_2 had to be found out by systematic experiments.

To find out the optimum annealing conditions, the samples were treated for different annealing temperature, annealing duration and annealing atmosphere. It was followed by beta irradiation dose of 1 Gy using $^{90}Sr/^{90}Y$ radiation source. The corresponding TL behaviour of the main dosimetric peak (~200 ˚C) was then recorded using Daybreak 2200 reader [8]. A constant heating rate of 1 ˚C/s was used throughout. All the readings were normalized for 1 mg. For each reading three discs were measured. The value of emitted photon count is average of the three and the error is standard deviation of these three measurements. A Schott bg39 broadband interference filter of 2 mm thickness was used in front of the photodetector. Its transmission curve is shown in figure 1.

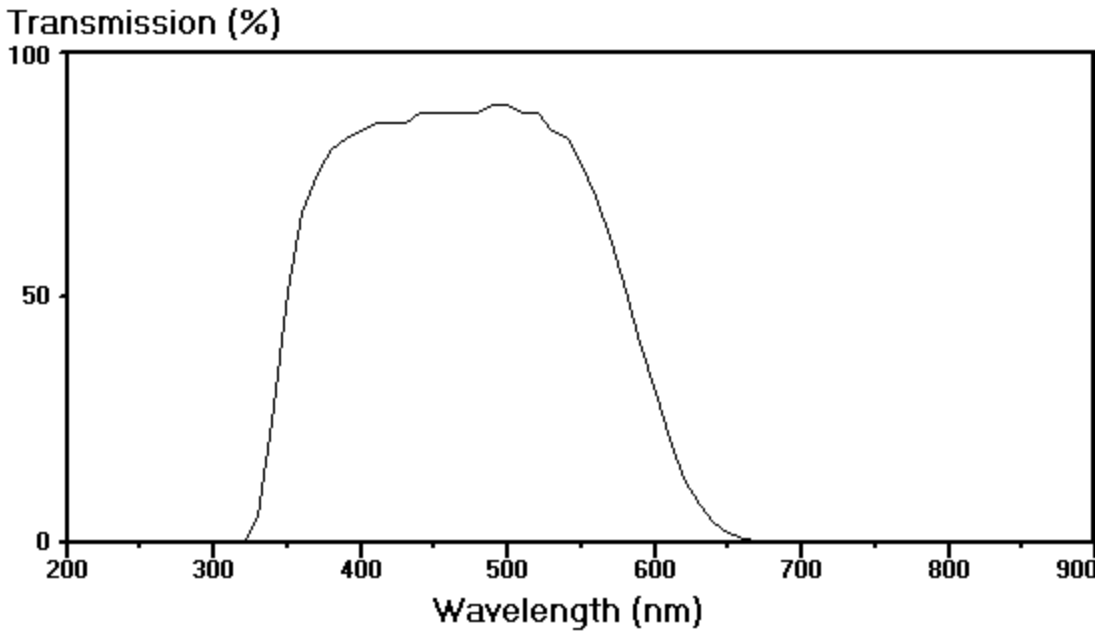

Figure 1. Transmission curve for Schott bg39 filter of 2 mm thickness.

5.2.1 Air versus vacuum annealing

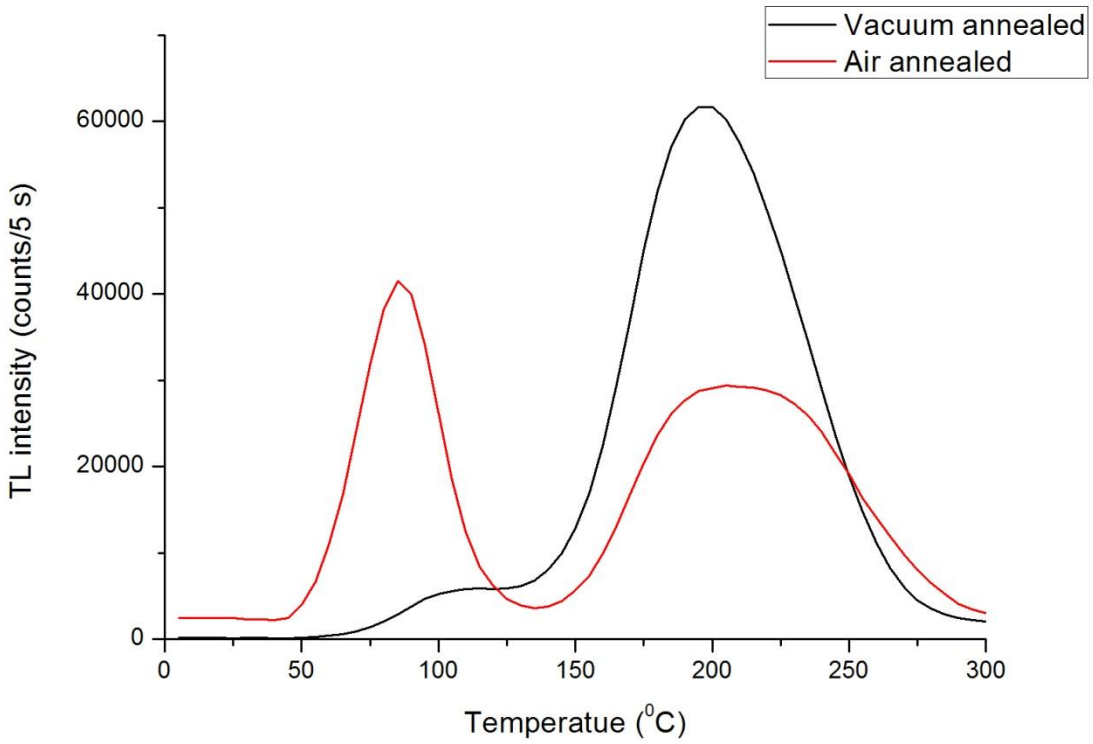

Figure 2: Glow curves of CaF_2 annealed in vacuum and in air

Annealing was done in vacuum at 95 kPa and in air at 500 ˚C for 1.5 h. Figure 2 shows the respective glow curves. The low temperature peak, being unstable, is not taken into consideration. The sensitivity of vacuum annealed CaF_2 was 1.64 times higher than the air annealed CaF_2. The sensitivity is calculated by integrating the counts of the glow curve peak at ~ 200 ˚C. Peak temperature indicates the location of traps. Shallow traps will correspond to lower peak temperature and deeper traps will correspond to higher peak temperature. FWHM of the glow curve peak indicates how closely the traps are spread out. Higher FWHM indicates broad distribution of peaks while lower FWHM indicates narrower distribution of peaks. FWHM of vacuum annealed CaF_2 was 73 ˚C and for air annealed CaF_2 it was 91 ˚C. Peak temperature T_m for vacuum annealed sample was at 195 ˚C and for air annealed it was at 205 ˚C. Thus it is confirmed that annealing in vacuum makes the material better crystalline than annealing in air since it has been suggested that lower T_m and FWHM along with higher sensitivity are an indication of the degree of crytallinity of the material [9-10].

5.2.2 Annealing temperature

Next, the annealing duration was fixed at 1.5 h and the annealing temperature was varied from 400 ˚C to 700 ˚C in the steps of 100 ˚C. Figure 3 shows the glow curves of nano-CaF_2 annealed at different temperatures for constant time duration of 1.5 h. The effect of annealing temperature on TL sensitivity (counts/mg/Gy), FWHM and T_m is shown in figures 4-6.

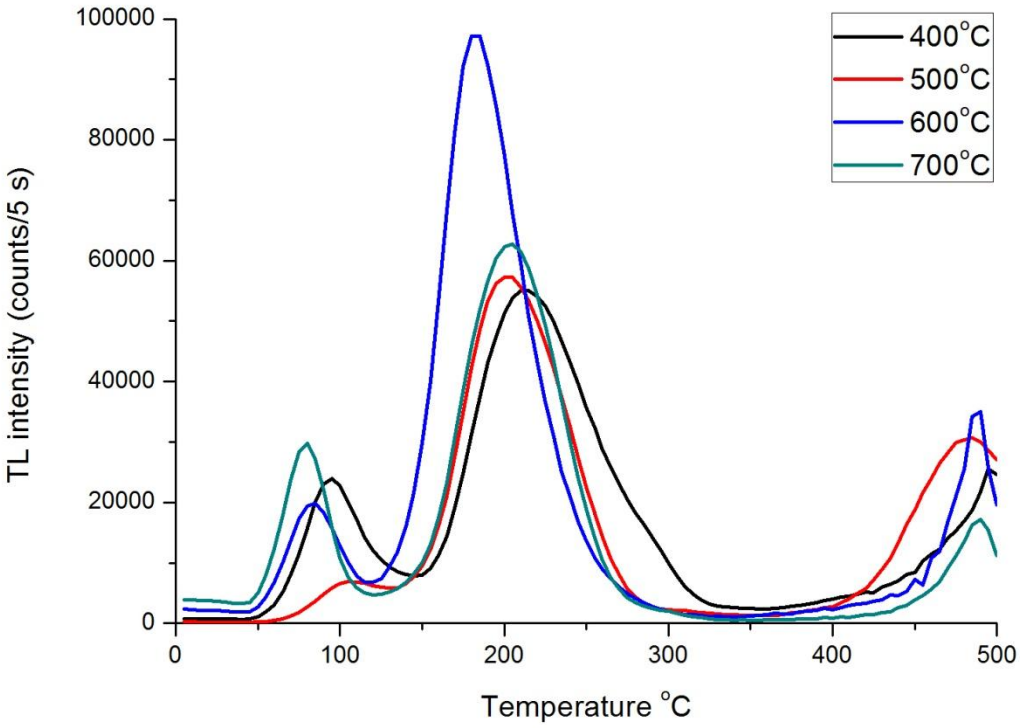

Figure 3. Glow curves of CaF_2 annealed at different temperature

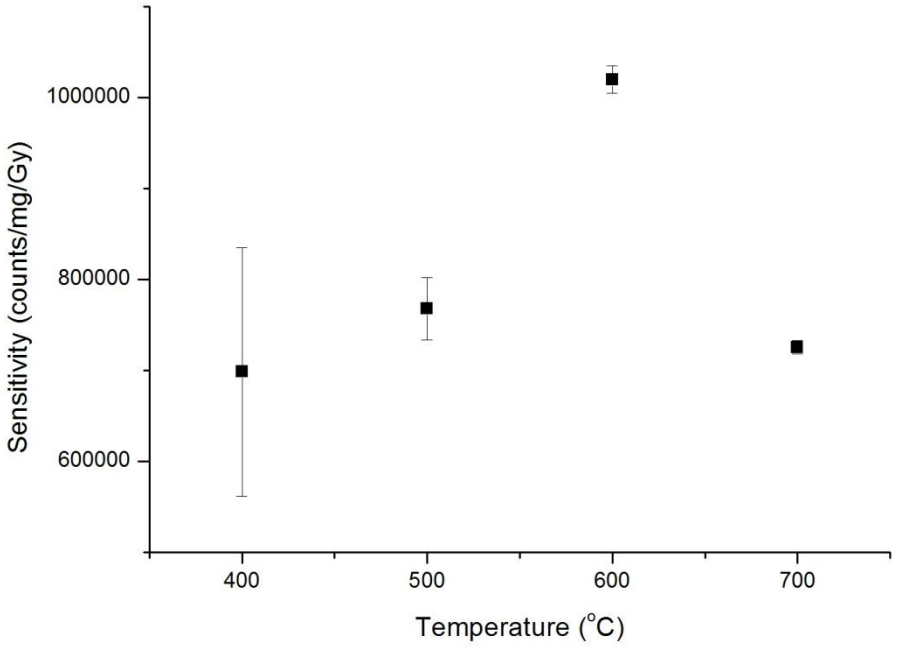

Figure 4. TL sensitivity of CaF_2 for different annealing temperature at a fixed annealing duration of 1.5 h

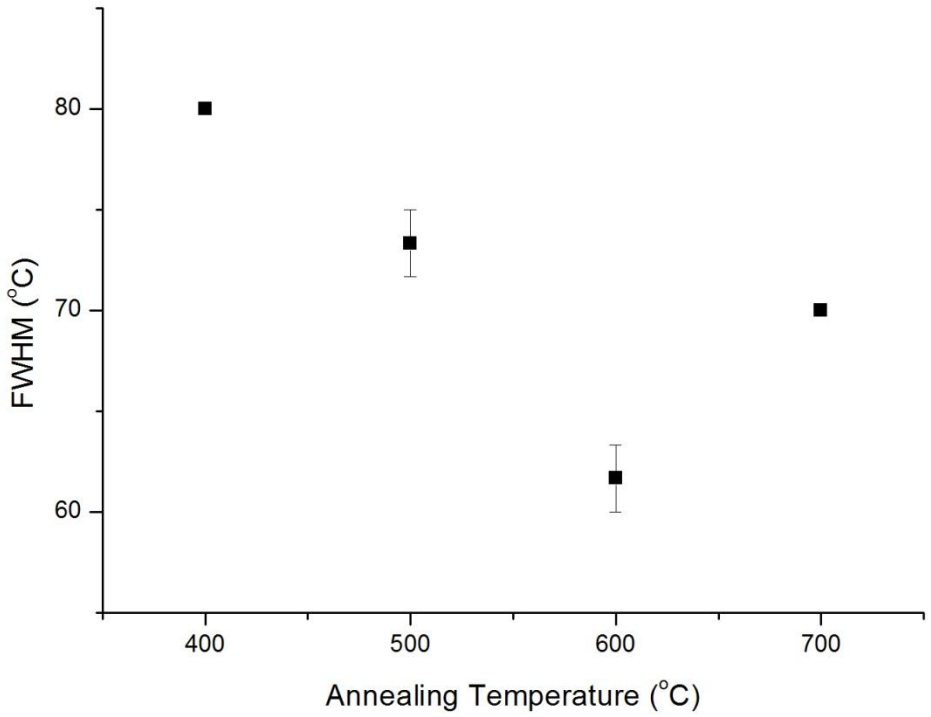

Figure 5. FWHM for different annealing temperature at a fixed annealing duration of 1.5 h

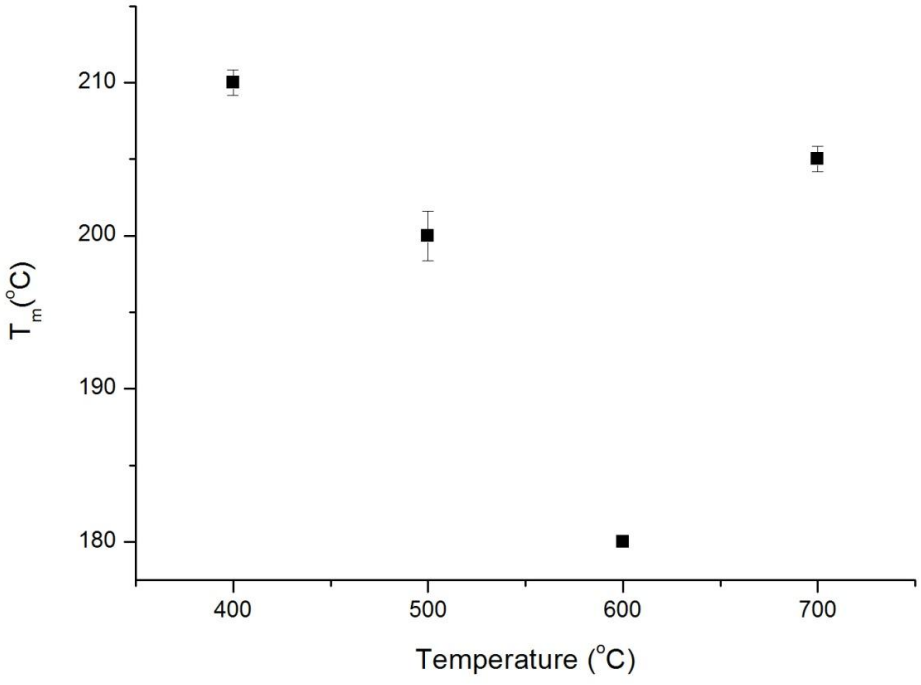

Figure 6. T_m with respect to different annealing temperatures for a fixed annealing duration of 1.5 h

From figures 4-6 it can be concluded that as the annealing temperature increases from 400 ˚C to 600 ˚C there is an increase in TL sensitivity, decrease in FWHM and shift of peaks towards the lower temperature region. A reversal in the trend is observed after 600 ˚C i.e. a decrease in TL sensitivity, increase in FWHM, and the shifting of peaks to the higher temperature region is observed after 600 ˚C. Thus 600 ˚C is the best annealing temperature when the annealing duration is of 1.5 h.

With respect to the pattern of change in sensitivity i.e. it increases till 600 ˚C and then decreases, similar observation was reported for CaSO4:Dy [11]. It was reported that peak temperature intensities increases as the annealing temperature increases from 400 ˚C to 600 ˚C after which there was a drastic reduction in the peak intensities. Their annealing duration was of an hour.

5.2.3 Annealing duration

Annealing duration was investigated for two temperature—600 ˚C and 500 ˚C. Sensitivity for 500 ˚C was found to be better than that of 600 ˚C as can be seen in figure 7. Temperatures below 500 ˚C were not explored because the TL was to be done till 500 ˚C. Temperatures above 600 ˚C were not explored because it was noted that with the increase in the temperature from 500 ˚C to 600 ˚C, the TL response deteriorated. It can be thus inferred that any further increase in the temperature would further deteriorate the TL response.

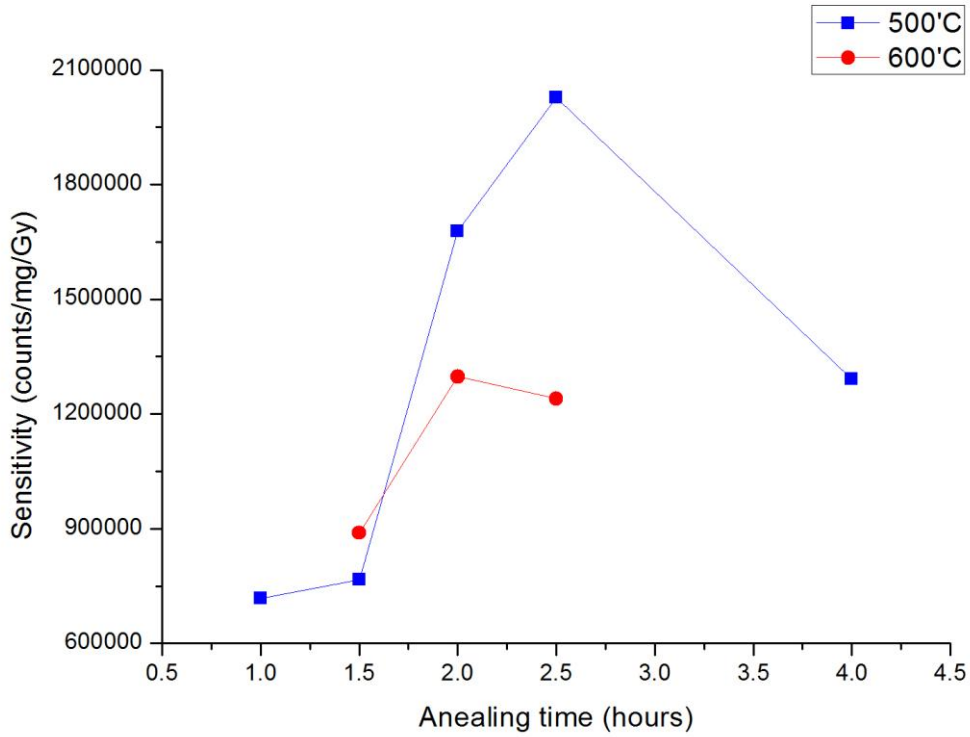

Figure 7. Annealing at various duration while keeping the temperature fixed at 500 ˚C and at 600 ˚C

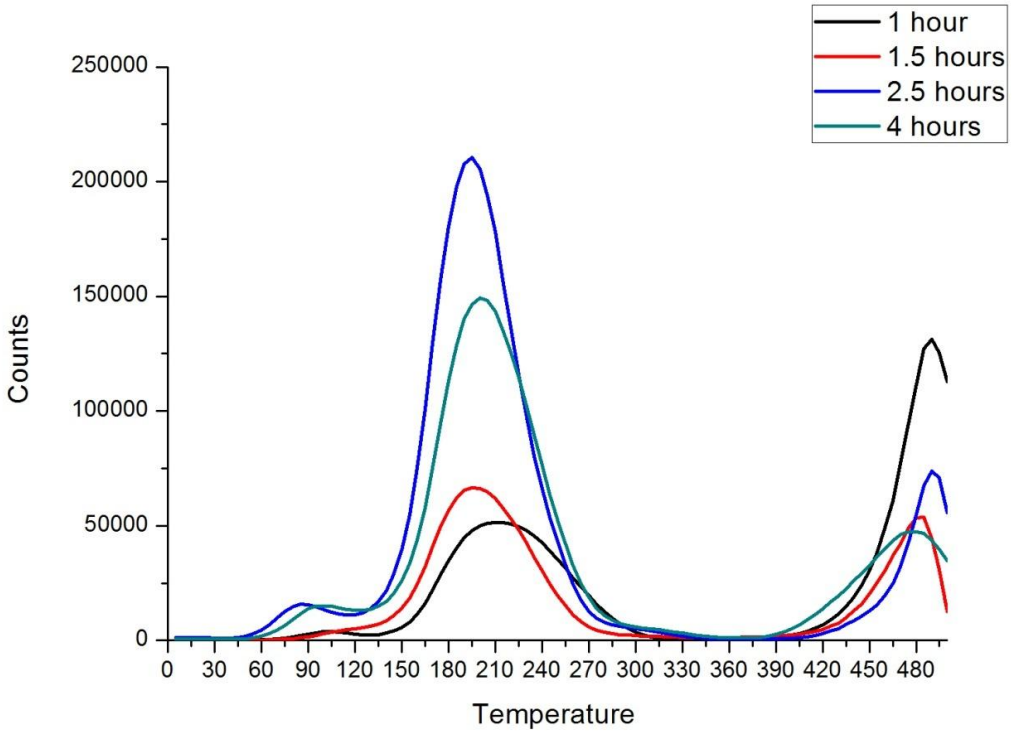

Figure 8. Glow curves for different duration of annealing for fixed temperature of 500 ˚C

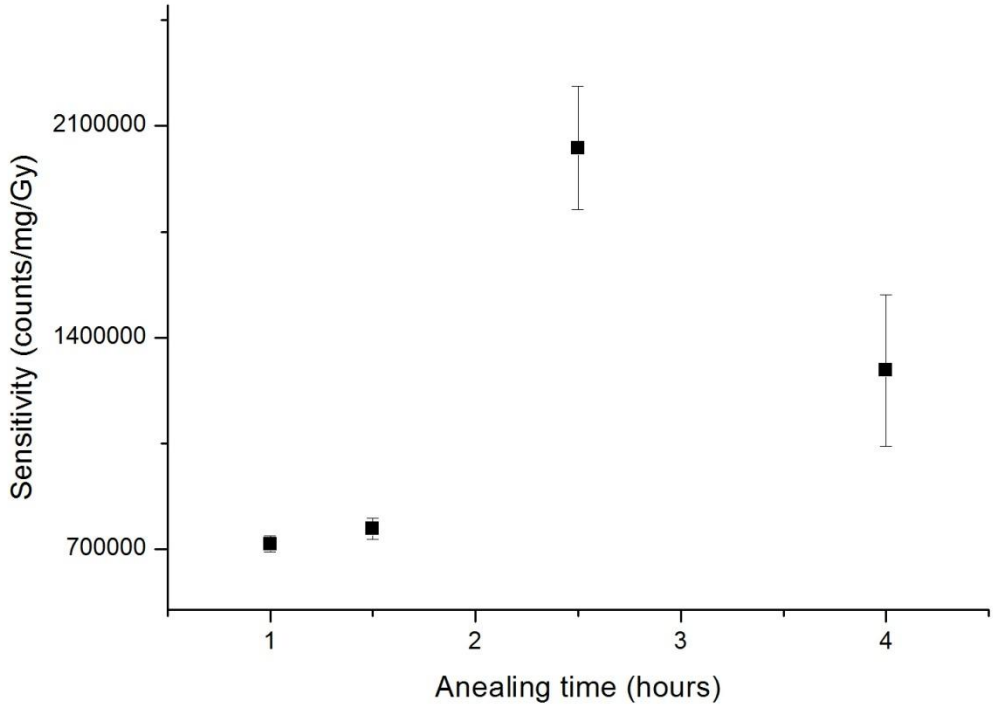

Figure 9. TL sensitivity for different duration of annealing for fixed temperature of 500 ˚C

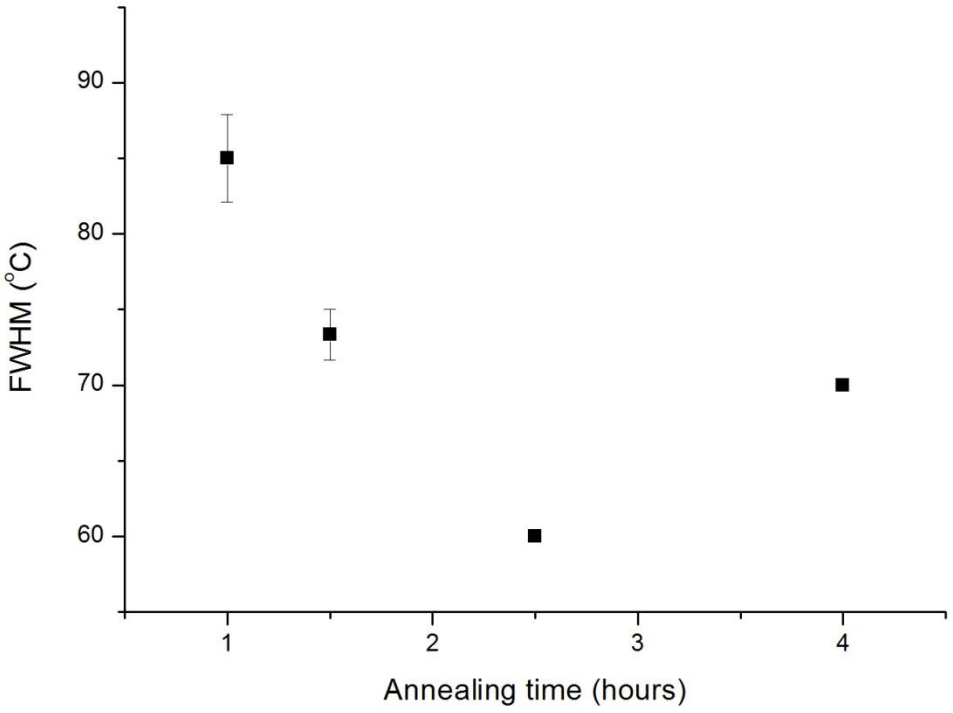

Figure 10. FWHM for different duration of annealing for fixed temperature of 500 ˚C

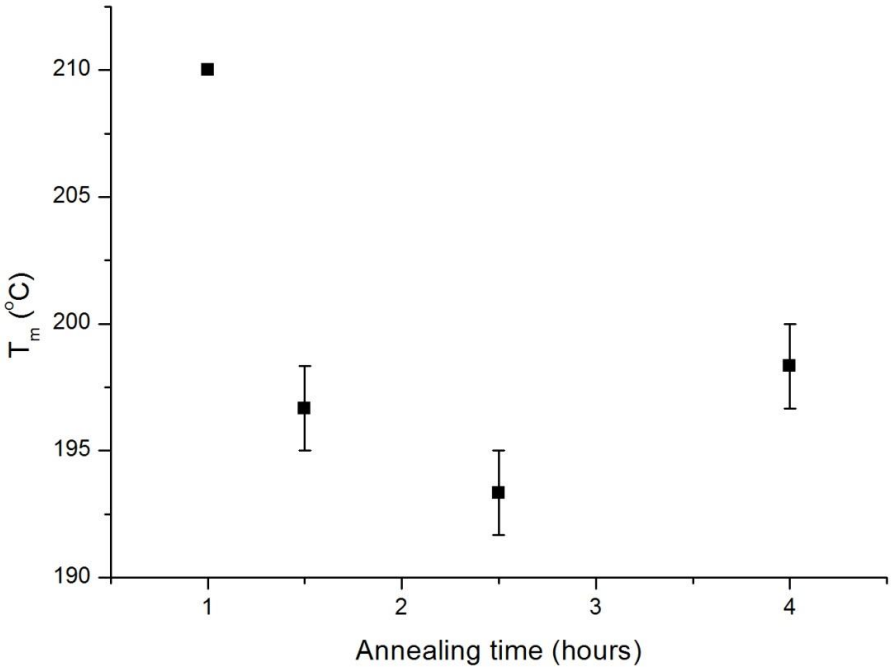

Figure 11. Peak temperature (Tm) for different duration of annealing for fixed temperature of 500 ˚C

Figure 8 shows the glow curves of nano-CaF_2 annealed at 500 ˚C for different durations. The effect of annealing duration on TL sensitivity, FWHM and T_m is shown in figures 9-11.

From figures 9-11 it can be concluded that as the annealing duration increases from 1 to 2.5 h there is an increase in TL sensitivity, decrease in FWHM and the peaks are shifted towards the lower temperature region. A reversal in the trend is observed after 2.5 h i.e. a decrease in TL sensitivity, increase in FWHM and the shifting of peaks to the higher temperature region. Thus 2.5 h of annealing duration with the annealing temperature of 500 ˚C is the best annealing condition for nano-CaF_2 to improve its TL properties.

5.3 Thermal Quenching

Thermal quenching is the process when the emitted light decreases due to non-radiative recombination of electrons and holes with the increase in temperature. In order to find the occurrence of thermal quenching, the glow curve of the sample is recorded for various heating rate.

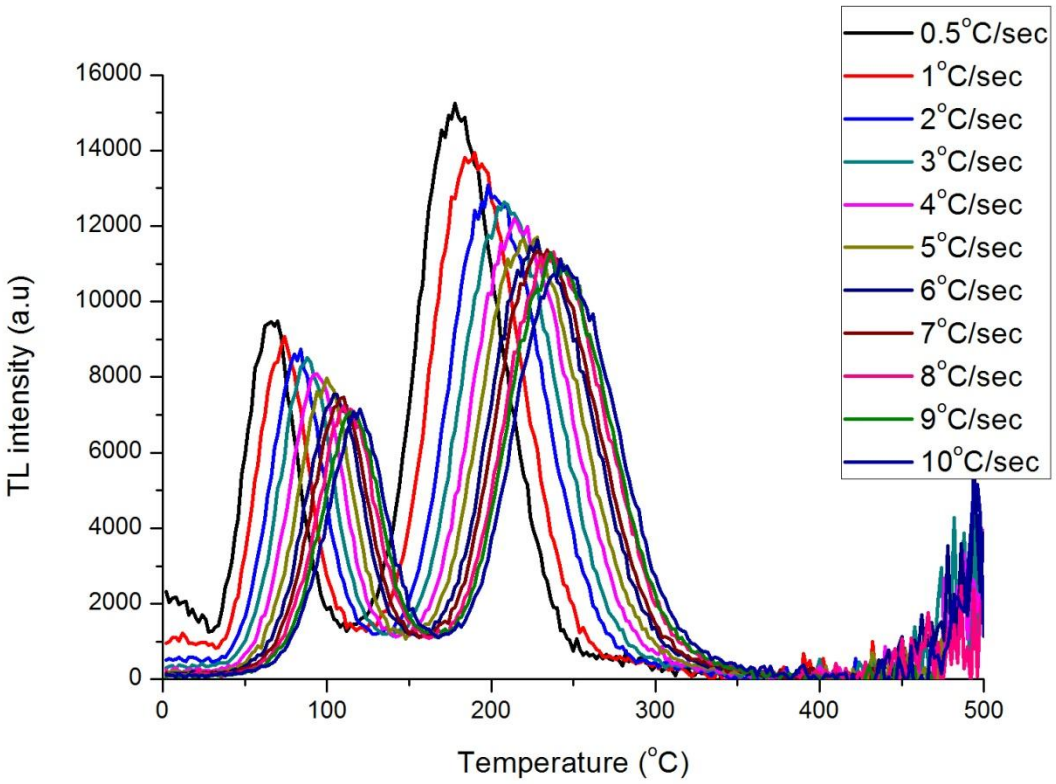

Figure 12. Effect of different heating rate on the glow curve

It is observed from figure 12 that with increasing heating rate, the peaks shift to higher temperature. The peak intensity decreases but peak width increases i.e. the total area under the curve remains the same. This implies absence of thermal quenching which causes decrease in the area under the curve with increase in the heating rate [12].

5.4 TL Characteristics

A TL phosphor can be characterised by parameters like order of kinetics followed by the phosphor, the activation energy which is also called trap depth, frequency factor *s*, etc. One of the primary aims of studying TL is to find out these parameters. They provide an insight into the underlying process governing the behaviour of the phosphor, though complete and sure understanding of the mechanism is still an active area of research.

5.4.1 Randall – Wilkins model

A mathematical model to describe thermoluminescence was first formulated by Randall and Wilkins [13]. According to this thermoluminescence model, the probability of re-trapping of electrons released from their traps is negligible as compared to the probability of their recombination. It was also assumed that the number of traps were much larger compared to the electrons in the conduction band. Thus it can be said that the luminescence intensity at any temperature is directly dependent on the rate of de-trapping of electrons which is proportional to the probability of the electrons escaping from their traps.

The probability of an electron escaping from a trap of depth E at temperature T is

$$p = s\exp\left(\frac{-E}{kT}\right) \qquad \text{.....(1)}$$

If n is the number of trapped electrons at time t, the change in n with respect to time is

$$\frac{dn}{dt} = pn = ns\exp\left(\frac{-E}{kT}\right) \qquad \text{.....(2)}$$

The thermoluminescence intensity is proportional to rate of supply of electrons to the luminescence centres.

$$I(t) = -\frac{dn}{dt} = -ns\exp\left(\frac{-E}{kT}\right) \text{.....(3)}$$

where

I(t) is the emission intensity,

n is the concentration of trapped electrons at time t (m^{-3}),

t is the time (s),

s is the pre-exponential (frequency) factor (s^{-1}),

E is the activation energy (eV),

k is Boltzmann's constant (eV/K) and

T is the absolute temperature (K).

The negative sign indicates that the density of trapped electrons decreases with time and temperature. The TL processes following this equation are said to be governed by the first order kinetics since the intensity of luminescence is proportional to n^1. The power of n determines the order of kinetics.

5.4.2 Garlick-Gibson model

The assumption of Randall and Wilkins [13] that the probability of re-trapping of electrons is negligible as compared to the probability of their recombination is not applicable in many cases. This lead to the suggestion of a new model of thermoluminescence by Garlick and Gibson [14]. They took into account the probability of re-trapping and to simplify the model assumed the re-trapping and recombination probability to be equal. In this case the emitted light intensity is given by equation 4:

$$I(t) = -\frac{dn}{dt} = \left(\frac{n^2}{N}\right) s \exp\left(\frac{-E}{kT}\right) \quad \text{.....(4)}$$

Where N is the total trap concentration (m^{-3}). The other terms are as previously mentioned.

The TL processes following this equation are said to be governed by the second order kinetics as the intensity of luminescence is proportional to n^2. Since the second order kinetics is due to the increased probability of re-trapping which causes a delay in luminescence, the second-half of the glow curve will be bigger than that of the first order glow curve. So the glow curves of the second order kinetics will be symmetric compared to the first order kinetics as shown in figure 13.

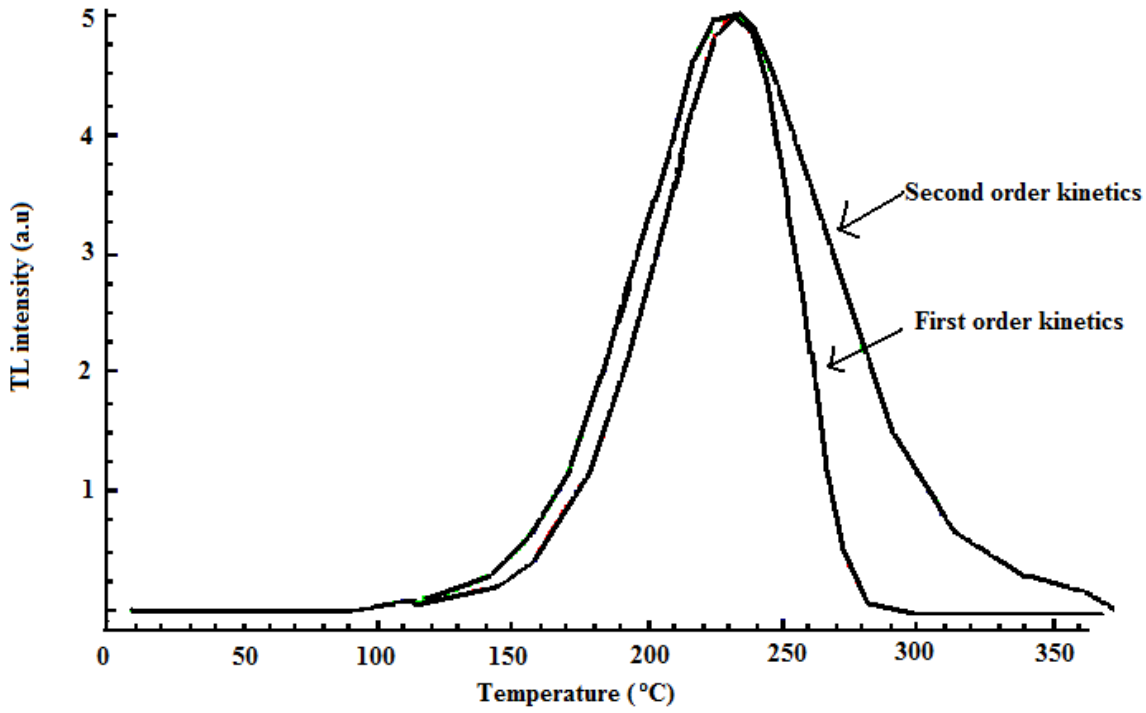

Figure 13. Difference between first order kinetic and second order kinetics glow-curve

5.4.3 General order kinetics

There are cases where the order of kinetics is found to be neither 1 nor 2. Many such instances are reported [15-19]. There might be a case where two electrons are trapped in the same trap. In such a case the order of kinetics may be 1.5 [20]. Such cases are said to follow the general order kinetics. The equation for the TL process governed by the general order kinetics is [15]

$$I(t) = -\frac{dn}{dt} = n^b s' \exp\left(\frac{-E}{kT}\right) \quad \text{.....(5)}$$

Where

b = the order of kinetics,

s' = s/N. It is called the effective pre-exponential factor for general order kinetics

The other terms are as previously mentioned.

5.4.4 Methods for determining TL parameters

A TL phosphor can be characterised by parameters like the order of kinetics (*b*), the activation energy (*E*), frequency factor (*s*), geometrical factor (μ), etc. Various methods like initial rise method, isothermal decay method, variable heating rate method, methods based on the shape of the glow curve, etc. can be used for evaluating the various parameters [21].

All the TL measurements to determine these parameters were done on Risø TL/OSL-DA20. Schott bg39 broadband interference filter of 2 mm thickness was used in front of the PMT. Black body radiation is significantly reduced by the use of this filter and the spectral range of the emission is limited to the spectral range of the filter. The transmission curve of this filter is given in figure 14.

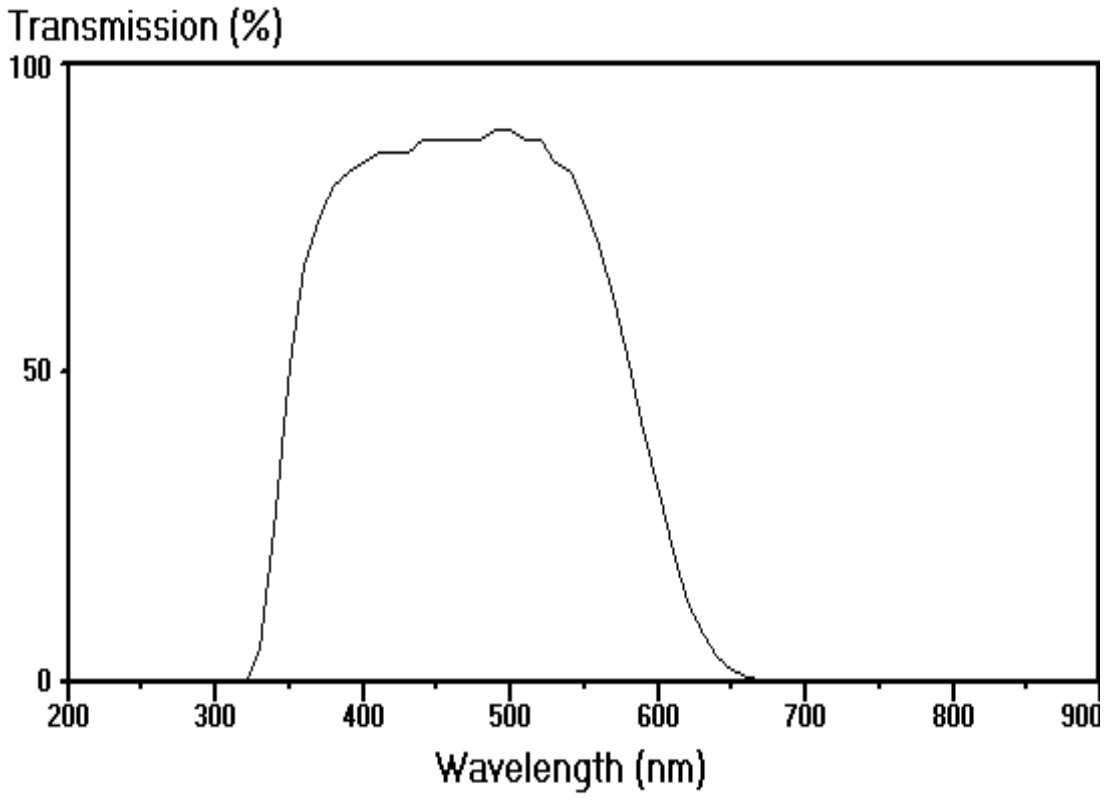

Figure 14. Transmission curve for Schott bg39 filter of 2 mm thickness.

5.4.4.1 Initial rise method

The initial rise method is used to calculate the activation energy and it is independent of the order of kinetics. It was pioneered by Garlick and Gibson [14]. In this method the initial part of the glow curve is used as in this region the amount of trapped electrons can be considered to be constant and its dependence on temperature is negligible. Here the luminescence intensity is directly proportional to $\exp\left(\frac{-E}{kT}\right)$. It is given by

$$I(T) = C\exp\left(\frac{-E}{kT}\right) \quad \text{.....(6)}$$

where C is a constant.

A plot of ln(I) vs. 1/kT over this initial region gives a straight line with slope –E which is the activation energy. Thus the activation energy is obtained without any knowledge of the frequency factor *s*.

Procedure for calculating activation energy by initial rise method

In order to calculate the activation energy using this method the steps mentioned below were followed:

- The sample was irradiated with a dose of 1 Gy.
- TL glow curves of the phosphor were recorded for 100 ˚C, 120 ˚C, 140 ˚C, 160 ˚C, 180 ˚C, 200 ˚C, 220 ˚C, 240 ˚C, 260 ˚C, 280 ˚C and 300 ˚C sequentially.
- All the TL data were plotted in a graph as shown in figure 15.
- The initial part of the graph where the intensity is $1/10^{th}$ of the maximum intensity is taken, eg. in the case of TL till 180 ˚C, the maximum intensity of the emitted luminescence occurs when the heating temperature is at 179 ˚C. The photon counts at this intensity is 58600 counts. Then the temperature is found where the count is 5860 i.e. $1/10^{th}$ of 58600. This temperature is found to be 140 ˚C.

- The counts (I) from 135 ˚C to 145 ˚C (T) are used to plot a graph of ln(I) vs 1/kT as shown in figure 16. Here *k* is the Boltzmann's constant and its value is 8.617332478 x 10^{-5} eV/K. The slope of this graph, 1.06 eV, is the activation energy for 160 ˚C.

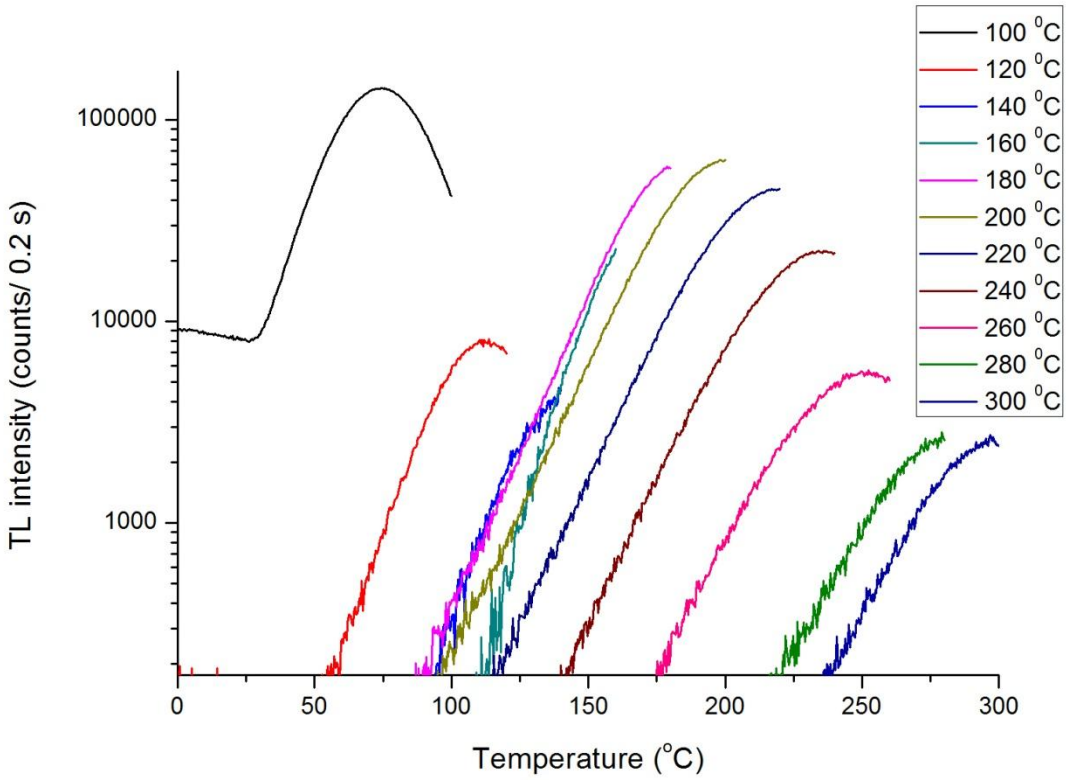

Figure 15. TL glow curve of the phosphor at sequentially increasing temperatures

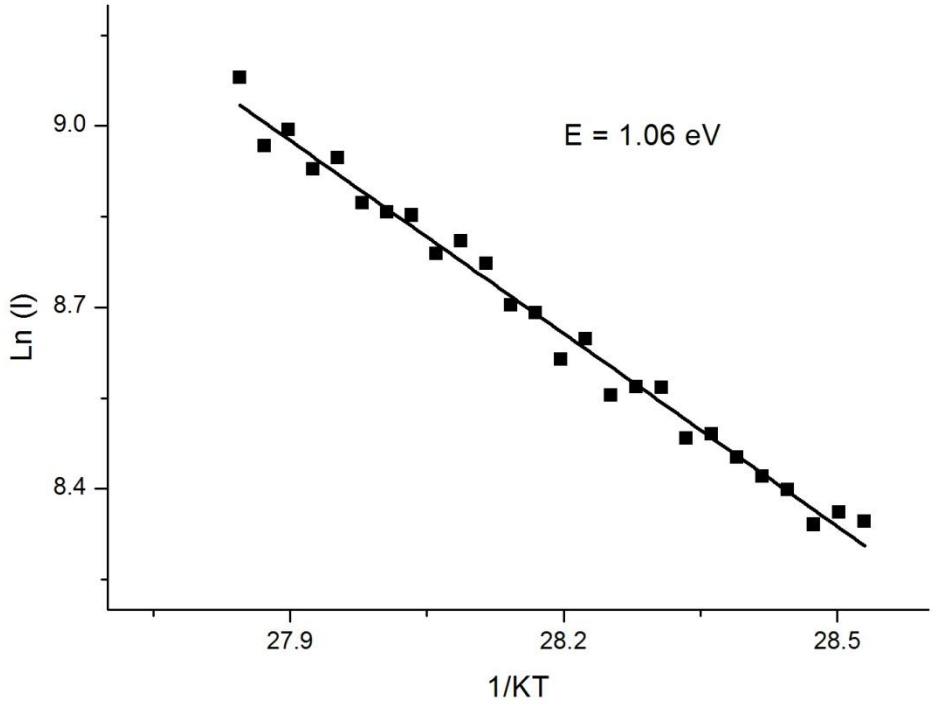

Figure 16. Graph of ln(I) vs 1/kT for TL up to 180 ˚C

- Similarly the graphs of ln(I) vs 1/kT for TL done till 200 ˚C and 220 ˚C are shown in figures 17 and 18 respectively. In the case of TL till 200 ˚C, the maximum count is 63300 and it occurs at 198 ˚C. $1/10^{th}$ of this count is 6330 and it corresponds to 160 ˚C. So counts (I) from 155 ˚C to 165 ˚C (T) are used to plot a graph of ln(I) vs 1/kT as shown in figure 17. Its slope is 1.03 eV.
- For TL till 220 ˚C the maximum count is 45400 and it occurs at 220 ˚C. $1/10^{th}$ of this count is 4540 and it corresponds to 165 ˚C. So counts (I) form 160 ˚C to 170 ˚C (T) are used to plot a graph of ln(I) vs 1/kT as shown in figure 18. Its slope is 1.06 eV.

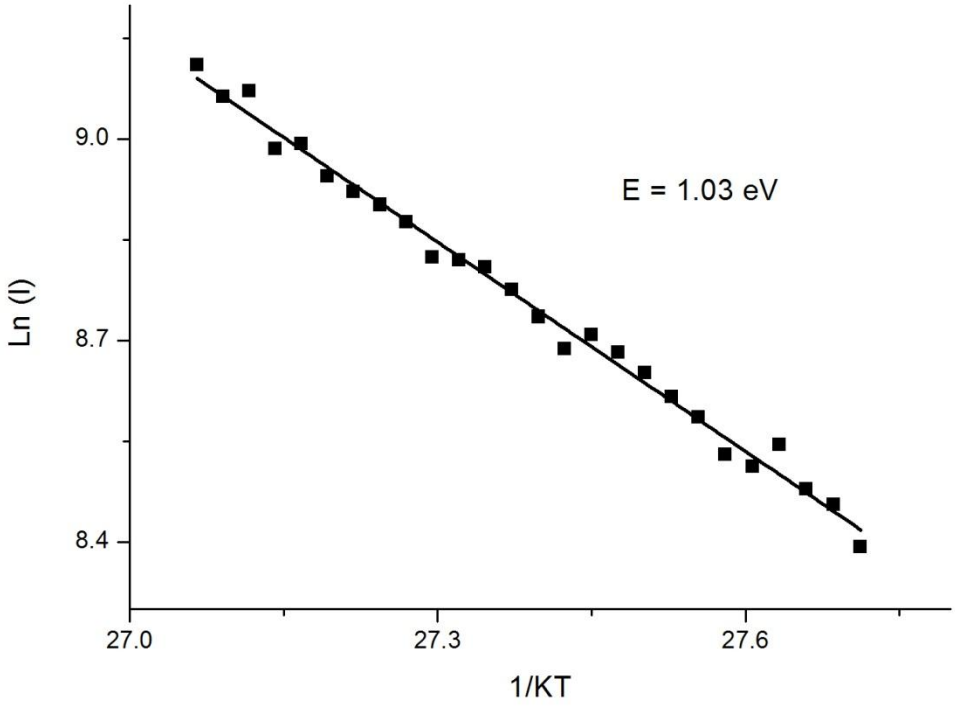

Figure 17. Graph of ln(I) vs 1/kT for TL up to 200 ˚C

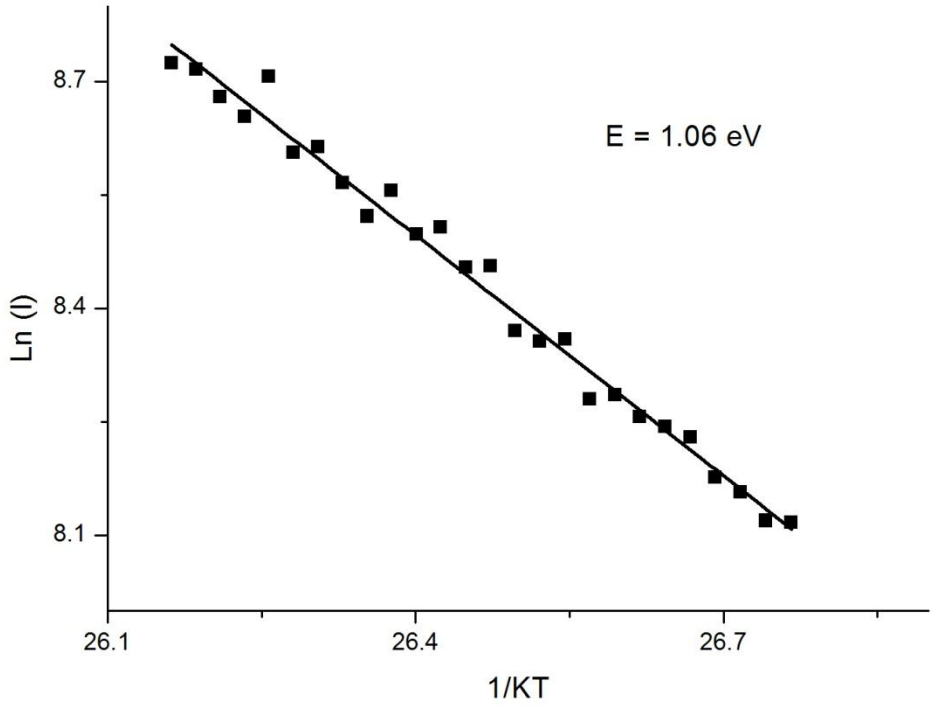

Figure 18. Graph of ln(I) vs 1/kT for TL up to 220 ˚C

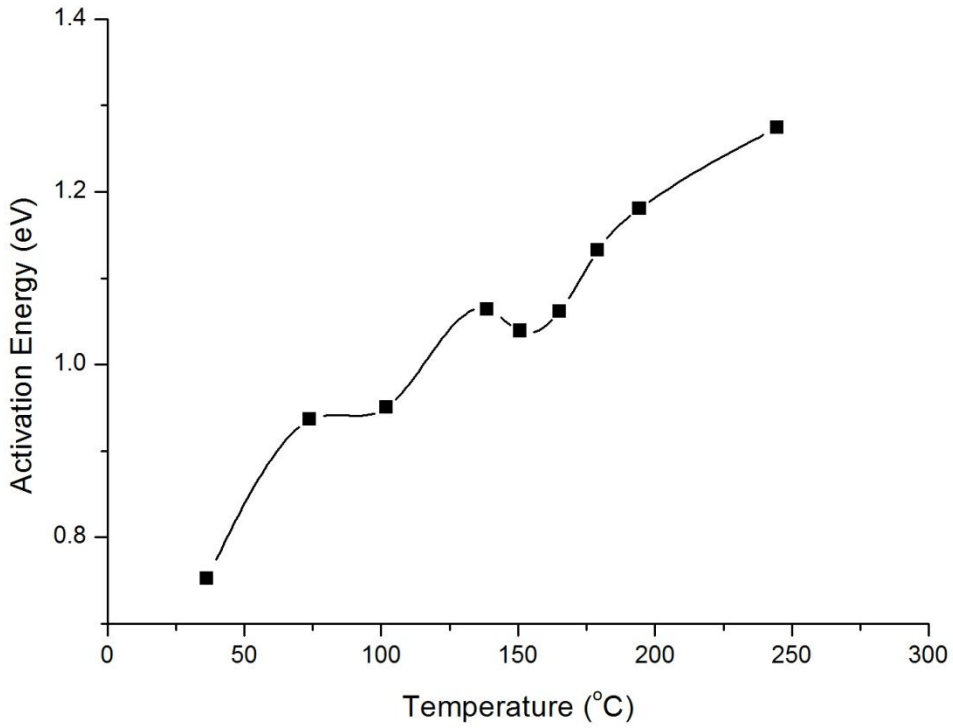

Figure 19. Activation energy at different temperatures

- The same process is done for all the eleven TL glow curves. So we get eleven activation energies corresponding to eleven temperatures. A graph of temperature vs activation energy is plotted as seen in figure 19. The part of the graph which corresponds to a straight horizontal line in the otherwise diagonal graph is the activation energy which is around1.04 eV

5.4.4.2 Method based on glow curve shape

In this method the kinetic parameters are deduced by examining the geometrical properties of the TL glow peak. As previously mentioned, the glow curve corresponding to the second order kinetics is more symmetric while the glow curve corresponding to the first order kinetics is more asymmetric.

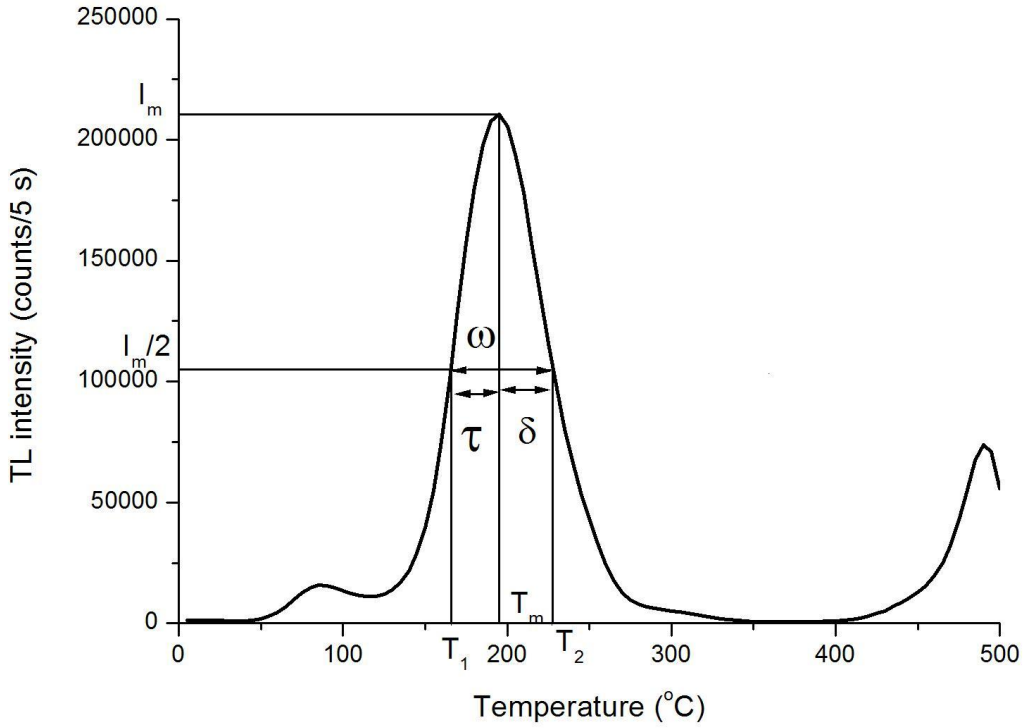

Figure 20. Geometrical parameters for the glow curve method of analysis

The parameters shown in Figure 20 are defined as follows:

T_m is the peak temperature

T_1 and T_2 are respectively the temperatures on either side of T_M, corresponding to half intensity

$\tau = T_m - T_1$ is the half-width at the low temperature side of the peak

$\delta = T_2 - Tm$ is the half-width toward the fall-off side of the glow peak

$\omega = T_2 - T_1$ is the total half-width

$\mu = \delta/\omega$ is the so-called geometrical shape or symmetry factor.

The above values calculated from the graph are as follows:

T_m= 193 ˚C,

T_1 = 165 ˚C,

T_2 = 227 ˚C,

τ = 28 ˚C,

δ = 34 ˚C,

ω = 62 ˚C,

μ = 0.54.

From the value of μ, the value of b is approximated to be 2.3. This is done from the graph calculated by Chen [9] of μ ranging from 0.36 to 0.55 for values of b between 0.7 and 2.5. This graph is redrawn in figure 21. Since the value of b is 2.3, it follows general order kinetics.

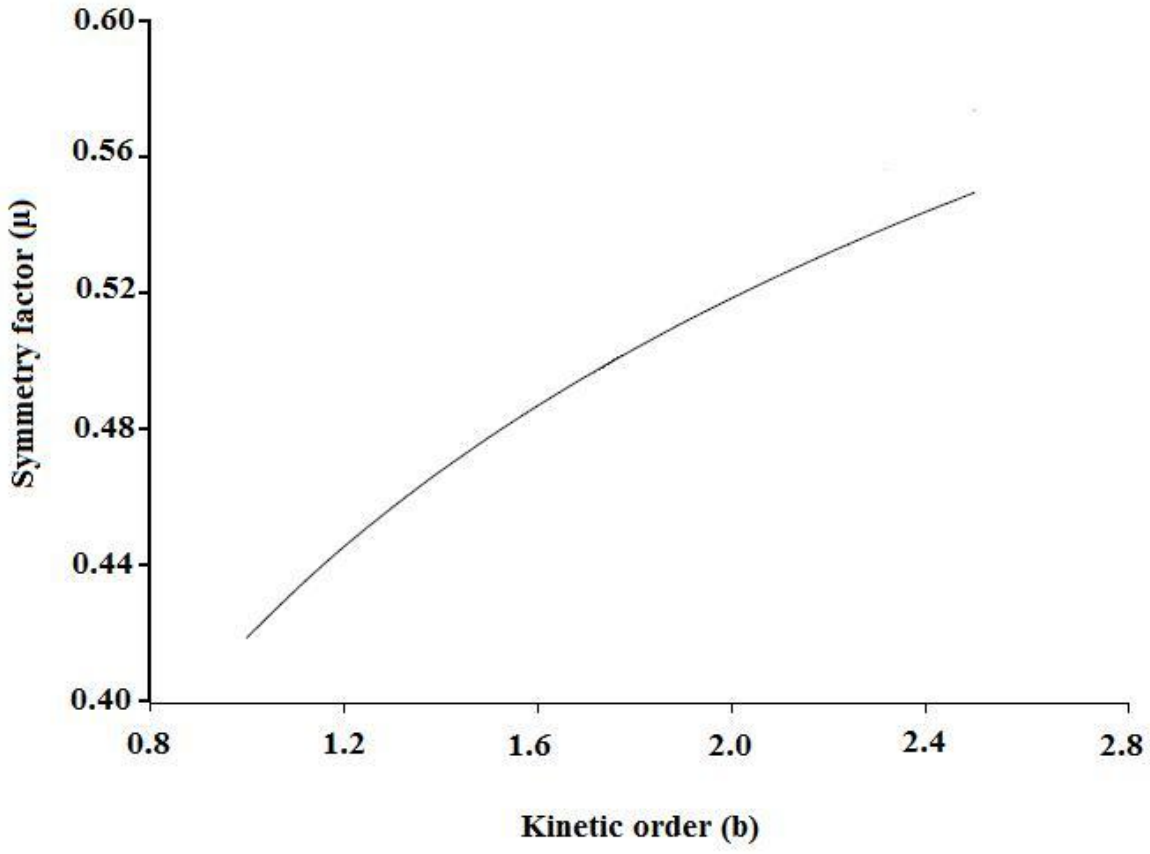

Figure 21. Relation between the symmetry factor (μ) and the order of kinetics (b)

For the general order kinetics, Chen's equation to find the activation energy is:

$$E_\alpha = c_\alpha \left(\frac{kT_m^{\,2}}{\alpha} \right) - b_\alpha (2kT_m) \quad \text{.....(7)}$$

Where α is τ, δ, or ω and the values of c_α and b_α are summarized below:

$c_\tau = 1.510 + 3.0(\mu - 0.42)$,
$b_\tau = 1.58 + 4.2(\mu - 0.42)$

$c_\delta = 0.976 + 7.3(\mu - 0.42)$,
$b_\delta = 0$

$c_\omega = 2.52 + 10.2(\mu - 0.42)$,
$b_\omega = 1.$

Calculation of E using the value of τ :

$c_\tau = 1.510 + 3.0(\mu - 0.42)$,
$= 1.510 + 3.0(0.54 - 0.42)$
$= 1.87$,

$b_\tau = 1.58 + 4.2(\mu - 0.42)$
$=1.58 + 4.2(0.54 - 0.42)$
$=2.084$

From the above two values E is calculated as:

$$E_\alpha = c_\alpha\left(\frac{kT_m^{\,2}}{\alpha}\right) - b_\alpha(2kT_m) \;\Rightarrow\; E\tau = c_\tau\left(\frac{kT_m^{\,2}}{\tau}\right) - b\tau(2kT_m)$$

$$= 1.87\left(\frac{8.6173324\times10^{-5}\times(193+273)^2}{(28+273)}\right) - 2.084\left(2\times8.6173324\times10^{-5}\times(193+273)\right)$$

$= 1.08$ eV

Calculation of E using the value of δ:

$c_\delta = 0.976 + 7.3(\mu - 0.42)$,

$= 0.976 + 7.3(0.54 - 0.42),$

$= 1.852,$

$b_\delta = 0,$

From the above two values E is calculated as:

$$E_\alpha = c_\alpha\left(\frac{kT_m^{\,2}}{\alpha}\right) - b_\alpha(2kT_m) \;\Rightarrow\; E_\delta = c_\delta\left(\frac{kT_m^{\,2}}{\delta}\right) - b_\delta(2kT_m)$$

$$= 1.852\left(\frac{8.6173324\times10^{-5}\times(193+273)^2}{(34+273)}\right) - 0$$

$= \quad 1.0193$ eV

Calculation of E using the value of ω:

$c_\omega = 2.52 + 10.2(\mu - 0.42),$

$= 2.52 + 10.2(0.54 - 0.42),$

$=3.744$

$b_\omega = 1.$

From the above two values E is calculated as:

$$E_\alpha = c_\alpha\left(\frac{kT_m^{\,2}}{\alpha}\right) - b_\alpha(2kT_m) \;\Rightarrow\; E_\delta = c_\omega\left(\frac{kT_m^{\,2}}{\omega}\right) - b_\omega(2kT_m)$$

$$= 3.744\left(\frac{8.6173324\times10^{-5}\times(193+273)^2}{(62+273)}\right) - \left(2\times8.6173324\times10^{-5}\times(193+273)\right)$$

$=1.049$ eV

5.4.4.3 Value of the activation energy from the peak temperature

Randall and Wilkins [13] derived the following equation for E:

$$E = T_M \{1 + f(s,\beta)\} k \log s \quad \text{.....(8)}$$

Here β is the heating rate. They observed that the peak temperature is only slightly affected by a change in the heating rate. The value of f (s,β) in equation 8 is very small compared to 1. They assumed *s* to be 2.9 x 10^9 s^{-1}. In such a situation, there is a relationship between the activation energy in eV and T_M in ˚k. This relationship is expressed by equation 9

$$E = 25kT_m \quad \text{.....(9)}$$

Using equation 9 the value of E was found to be 1.003919 eV

Urbach [22] also derived a similar equation (equation 10) assuming s to be 10^9 s^{-1}.

$$E = T_m/500 = 23kT_m \quad \text{.....(10)}$$

By the use of equation 10 the value of E was found to be 0.932 eV

5.4.4.4 Various method of variable heating rate

Many different methods of determining the kinetic parameters using variable heating rate have been proposed. Bohum *et al* [23], Porfianovitch *et al* [24] and Booth *et al* [25] proposed methods suitable for first order kinetics, which required two different heating rates. Chen and Winer [26] presented a method valid for any order of kinetics.

As can be seen from figure 22, with the increase in heating rate there is a shift of the peak temperature towards higher temperature region. In such cases the following equation for general order kinetics given by Chen and Winer [26] can be used.

$$\left(\frac{\beta}{T_M^2}\right) \cong \exp\left(-\frac{E}{kT_M}\right)\left(\frac{ks}{E}\right)[1+(b-1)\Delta_M] \quad \text{.....(11)}$$

Where $\Delta_M = 2kT_M/E$. The plot of $\ln\left(\frac{\beta}{T_M^2}\right)$ versus $\frac{1}{kT_M}$ is a straight line with slope $-E$.

This graph is plotted in figure 23. The activation energy was found to be 1.006 eV.

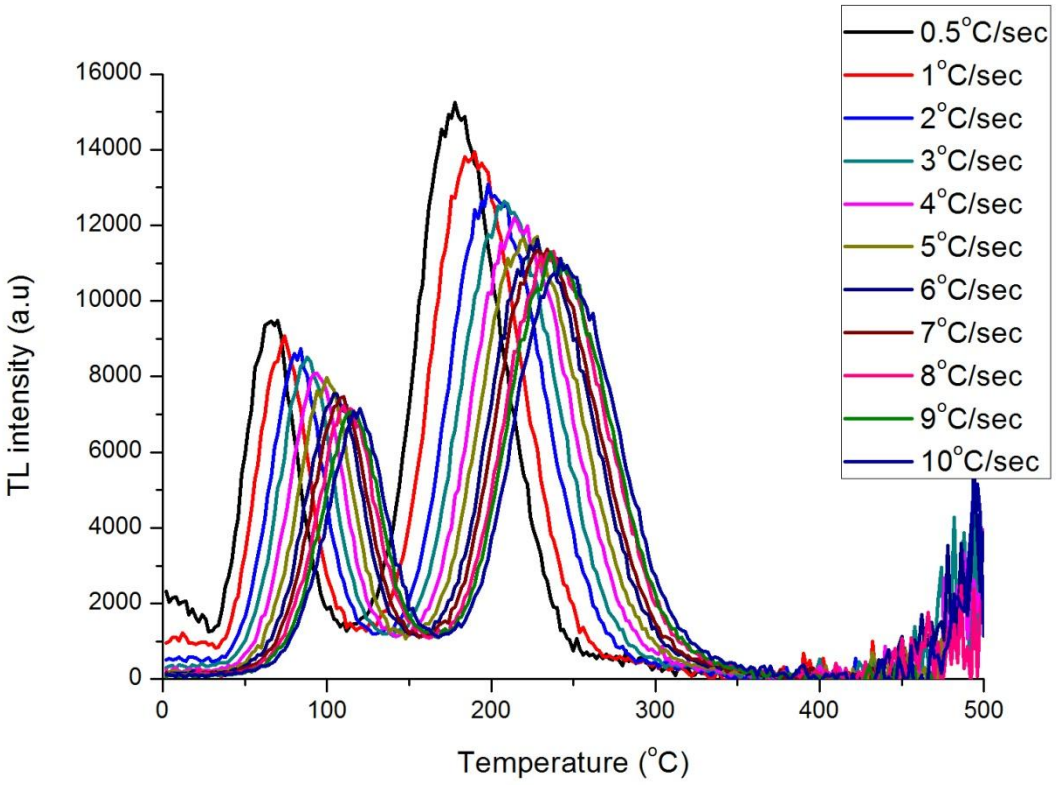

Figure 22. Effect of various heating rate on the glow curve

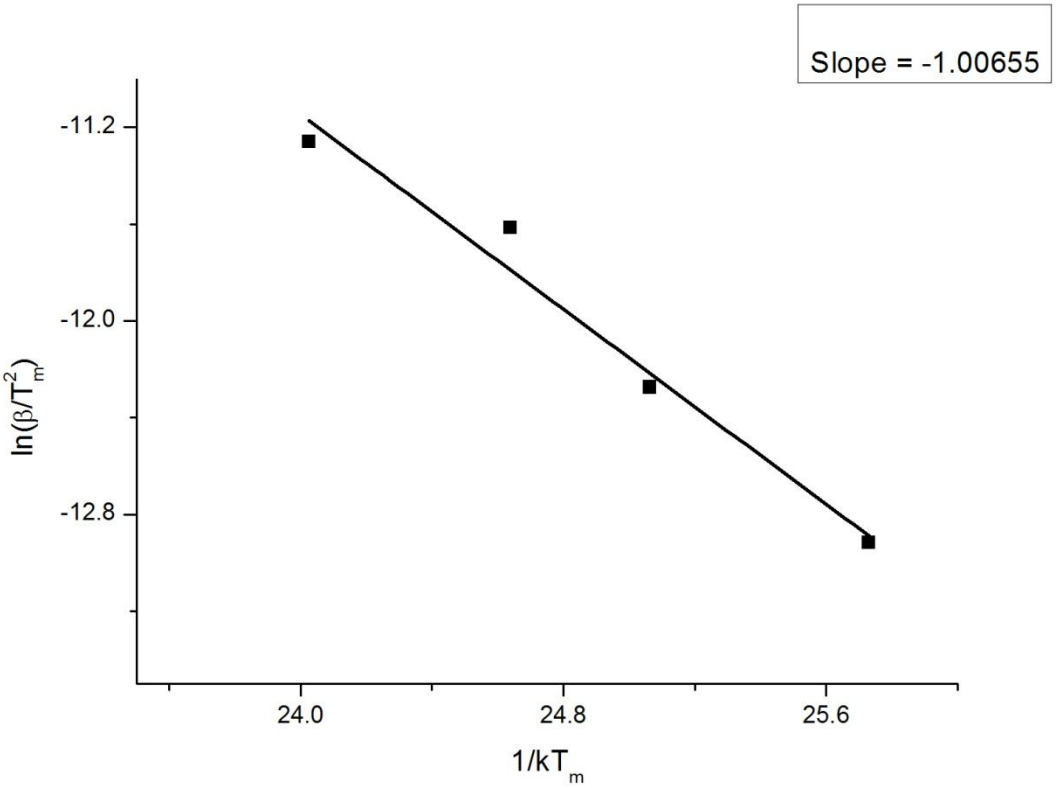

Figure 23. Graph of $\ln\left(\frac{\beta}{T_M^2}\right)$ versus $\left(\frac{1}{kT_M}\right)$ to calculate the activation energy

5.4.5 TL dose response and minimum detectable dose

Dose response of a phosphor gives the relation between the amount of dose that the phosphor was subjected and its emitted luminescence. TL is regularly being used for routine dosimetry in nuclear plants and research labs. Its use for dosimetry was developed form the early 1950s onwards.

The dose response of the prepared phosphor is given in figure 24. It gives a linear dose response till the dose of ~600 Gy. Beyond this point the TL response increases nonlinearly with dose. The dose response curve was fitted to the following single saturation exponential.

$$I = I_0\left[1-\exp\left(\frac{-D}{D_0}\right)\right] \quad \ldots\ldots\ldots\ldots\ldots\ldots\ldots\ldots\ldots\ldots\ldots\ldots\ldots\ldots\ldots\ldots(12)$$

Where,

I = measured intensity

I_0 = saturated intensity at infinite dose

D = given dose

D_0 = dose where the saturation begins (figure 24). Its intensity is 63% of the saturation intensity.

The graph for equation 12 is given in figure 25 which shows the dose saturation of the phosphor. The maximum detectable dose is $2D_0$. At this dose the signal intensity is 86% of saturation intensity. The calculated D_0 is 1026 Gy. So the maximum detectable dose ($2D_0$) is 2052 Gy.

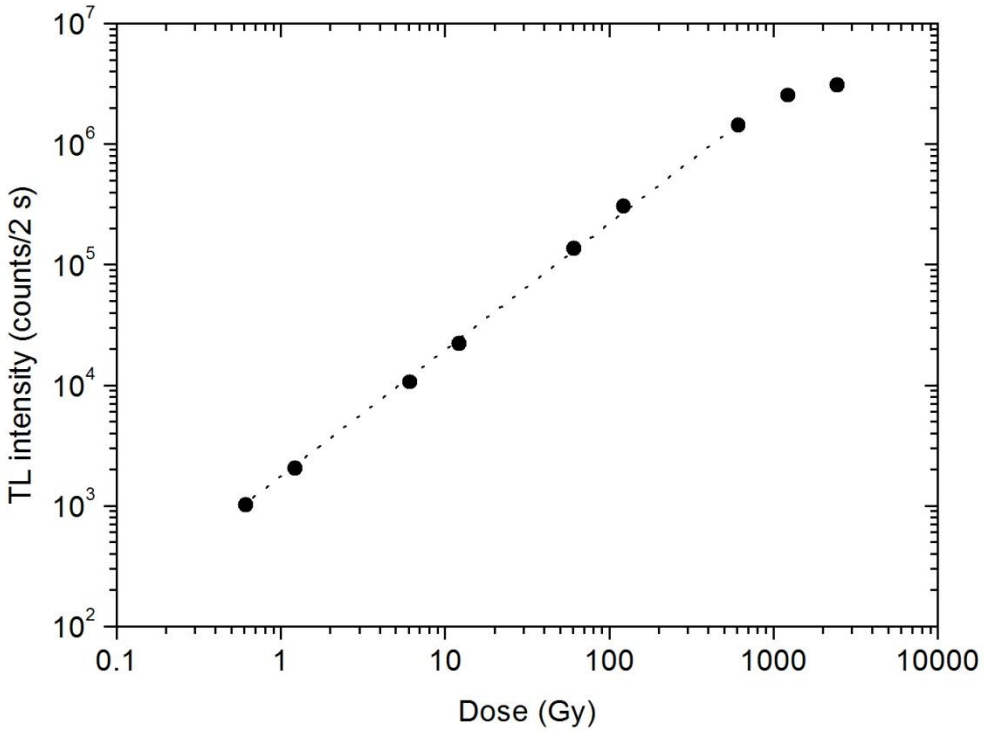

Figure 24. TL dose response of CaF_2

In order to find the minimum detectable dose, the sample has to be given doses in increasing order form the least possible dose to a level where meaningful response is obtained from the sample. Due to the limitation of the machine, the least possible dose that could be given was 0.05 Gy. It was given to a sample weighting 0.55 mg. The glow curve peak of this sample

corresponded to 3739 counts. The integration time of the detector was 5 s. It implies that 750 counts/s were obtained at the glow curve peak for the given dose. The photon counting system, comprising of the photo multiplier tube (PMT) and the associate electronics has a typical random fluctuation of 50 counts/s (also called noise). In order to get a meaningful measurement the signal should be greater than 150 counts/s. Since 0.55 mg of phosphor gave 750 counts/s for 0.05 Gy, 150 counts/s will be emitted from 1 mg of phosphor for 5 mGy. [750/5 = 150 (which is the meaningfully detectable counts), so 0.05/5 = 0.01 Gy for 0.55 mg. For 1 mg it will be 0.01/2 = 0.005 Gy or 5 mGy]. Thus 1 mg of present phosphor should be able to measure a minimum dose of 5 mGy, assuming linear dose response at low dose range.

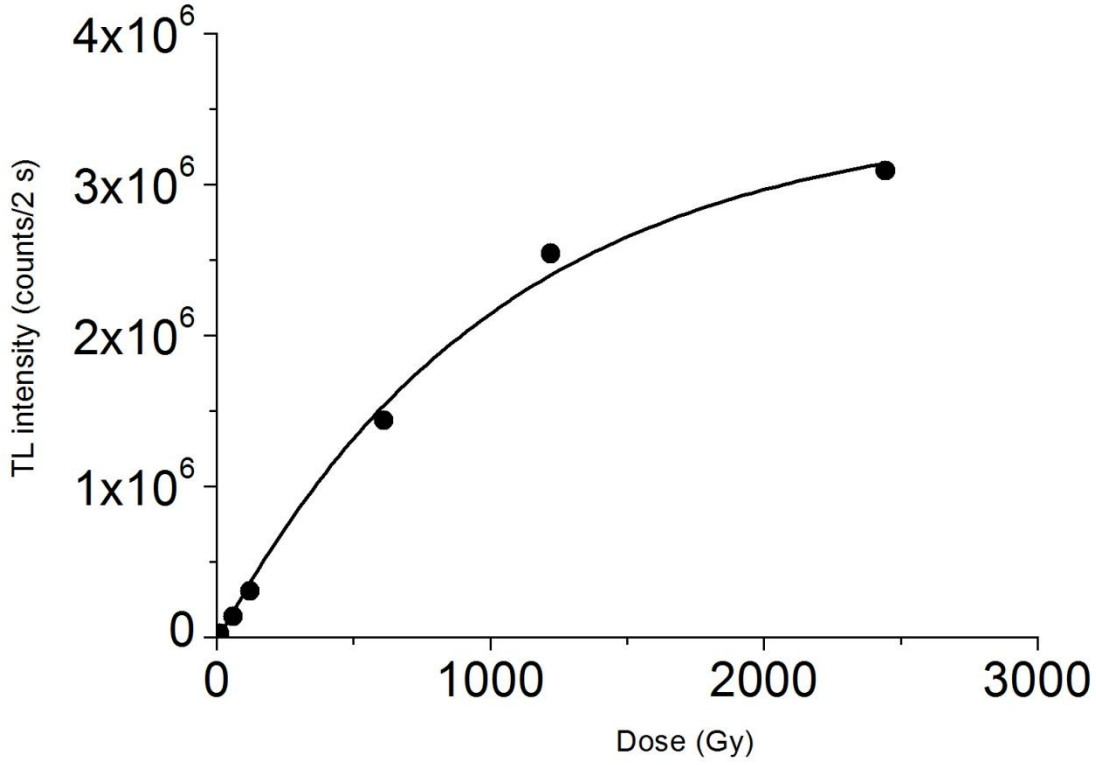

Figure 25. Saturation exponential, $I = I_0\left[1-\exp\left(\frac{-D}{D_0}\right)\right]$

5.4.6 Mechanism of TL in CaF_2

Since the TL properties of CaF_2 is enhanced by adding rare earth dopents or Mn, most of the reported literature on CaF_2 explains the luminescence as occurring due to the dopents. Merz *et al* has explained the TL emission of CaF_2 doped with RE^{3+} dopants [27]. The electrons released by the irradiation are captured by the impurity RE^{3+} ions, reducing them to RE^{2+}. The corresponding holes which are produced due to the release of electrons are captured by the host related defect centers as the modified V_k centre [28]. Due to the stimulation by heat these holes are successively released at different temperatures. The recombination of the released holes with the reduced RE ion causes luminescence. Due to this recombination RE^{2+} returns to its original state RE^{3+} in an excited state. Its relaxation to the ground state gives rise to luminescence. This process is depicted in the following table [28]

During irradiation	$RE^{3+} + e^- \rightarrow RE^{2+}$
	$F^- + \text{hole} \rightarrow V_k$
During stimulation	$V_k \rightarrow F^- + F^- + \text{hole}$
	$RE^{2+} + \text{hole} \rightarrow RE^{3+}$ (excited state) $\rightarrow RE^{3+} + TL$

Table 1.Charge conversion process of the centres involved in TL emission

In natural CaF_2, the luminescence is explained by stating that natural CaF_2 has some impurities in it which causes the luminescence. In the case of the synthesized CaF_2, the luminescence could be due to the defects caused due to the annealing treatment. Before annealing the material was not showing any TL but after annealing it showed TL. So we could infer that during the annealing process some defect creation or structural changes could have taken place which has caused it to have TL characteristics.

Alternativly the above model suggests the presence of F^- center in the bulk of CaF_2. The F^- center combines with the hole that is generated due to irradiation and gives V_k center. During stimulation the V_k center again gives a hole as suggested in the model. The hole combines with the electron which was formed dutring the electron-hole pair generation due to irradiation giving luminescence.

5.5 Optically stimulated luminescence

In OSL, the sample is first subjected to radiation due to which electron – hole pairs are formed. The electrons get trapped in the defects of the material. Then this sample is subjected to optical stimulation. Due to the optical stimulation the electrons get sufficient energy to escape from their traps, travel to the recombination centers through the conduction band and combine with holes emitting luminescence in the process.

5.5.1 Optical stimulation

The photon emission is very much dependent on the intensity and wavelength of the stimulating wave. It is possible that the emitted luminescence be of higher energy than that of the stimulating one. This happens because the emission characteristics are governed by the recombination centre. It depends on the transition of the electron from the excited state in the conduction band to the ground state at the recombination or luminescence centre. Thus it is perfectly possible that the stimulating wave may be in the blue region and the emission is in the UV region and this has been observed in many cases and also in the case of the synthesised CaF_2.

The intensity of the emitted luminescence is also strongly dependent on the intensity of the stimulating wave. For higher intensity stimulation, the trapped charges will be de-trapped at a faster rate, leading to higher intensity of the emitted luminescence. The emitted intensity may be linearly dependant on the stimulation intensity as is the case with Al_2O_3:C and BeO or it may be non-linearly dependant on the stimulation intensity as seen for NaCl [29].

5.5.2 Modes of OSL

Basically three modes of optical stimulation are used. In the continuous wave OSL (CW-OSL) mode the stimulating light is kept at a constant intensity and the emitted luminescence is measured. Appropriate filters are used so that the light detector detects only the emitted luminescence and not the stimulating light. It is the simplest and most commonly used mode. This mode is shown in figure 26.

In the linearly modulated OSL (LM-OSL) mode the intensity of the stimulating light is linearly increased and the emission is measured under this condition. Here also appropriate

filters are need to prevent the stimulating light from reaching the light detector. This mode is shown in figure 27.

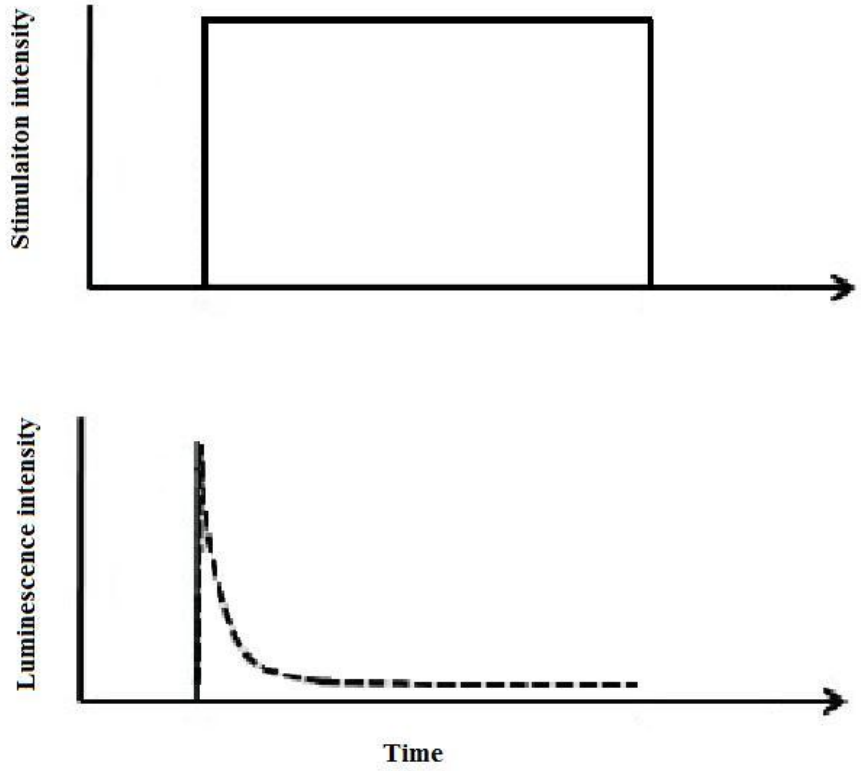

Figure 26. CW-OSL mode stimulation and emission

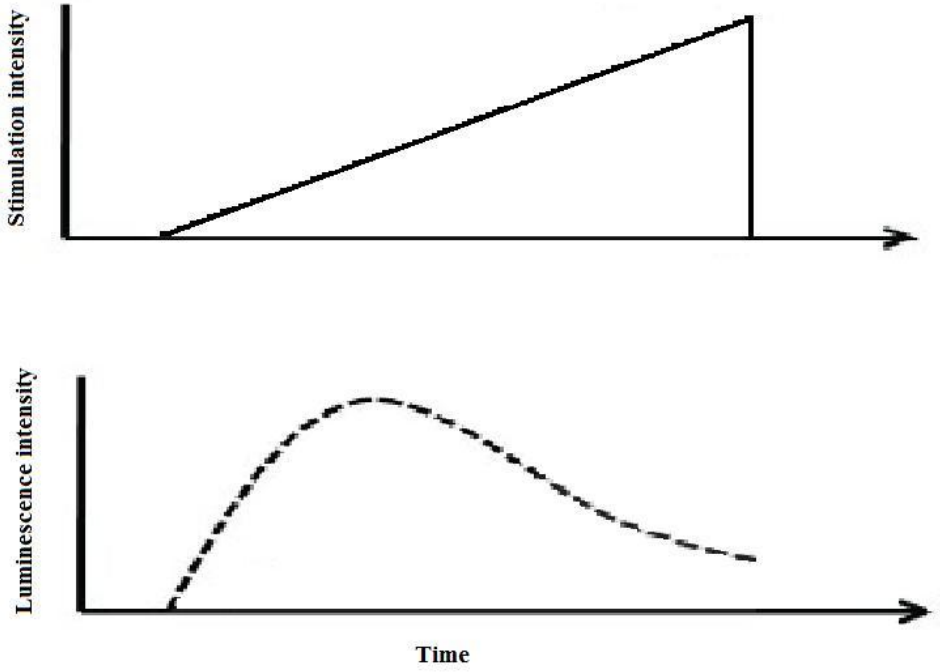

Figure 27. LM-OSL mode stimulation and emission

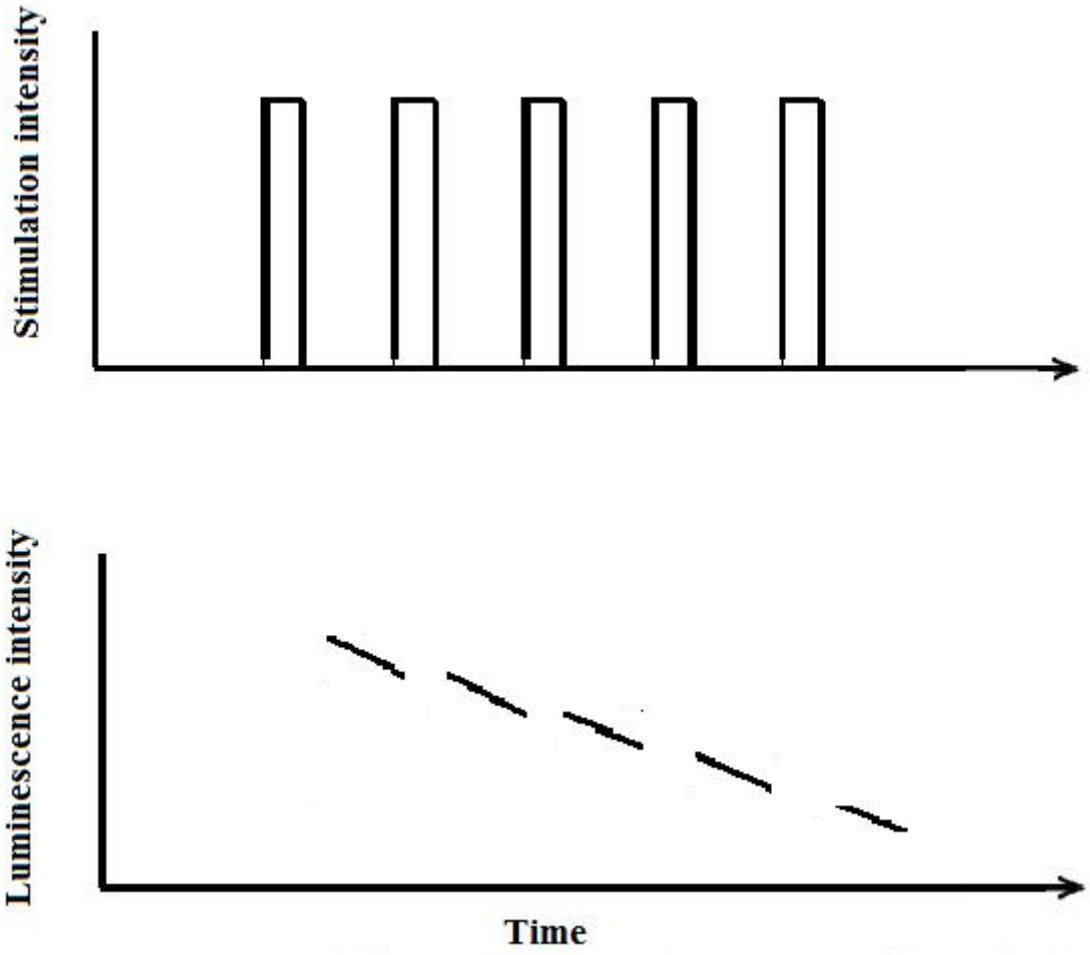

Figure 28. POSL mode stimulation and emission

The drawback of the CW-OSL and LM-OSL is that the stimulating light has to be of much higher wavelength to prevent the stimulating light passing through the filter and getting detected. The intensity of the emitted luminescence is also significantly attenuated by the filters which is not desirable in cases of very dull samples for geological dating or in the case of dosimetry, to measure very low level doses. This problem is solved in the pulsed OSL (POSL) mode. In this mode the light intensity is given in a pulsed manner and the emission is measured only when the stimulation is in the off state [30, 31]. By this procedure only the afterglow is measured. In this mode filters are not needed since the photon detection takes place only when the stimulating source is in the off state. Due to this the stimulating source can be of wavelength very close to that of the emitted luminescence. This mode is depicted in figure 28.

Other than the modes described above there are also modes of OSL such as delayed OSL (DOSL), photo-transferred OSL (PTOSL) and cooled OSL (COSL). Mathematical descriptions of optically stimulated luminescence (OSL) signals under linearly, hyperbolically, exponentially and reciprocally increasing stimulation intensity have been reported by Bos *et al.* [32]. Variable decay OSL (VD OSL) has been reported by Biernacka *et al.* [33]. All the above modes of OSL are also performed at elevated temperature in order to assist the OSL process or to remove contribution to emitted luminescence from shallow traps.

5.5.3 OSL Emission characteristics of the synthesised CaF_2

CaF_2 has been reported to be extremely sensitive to light, but very few studies have been done on its OSL properties [34, 35]. The synthesised CaF_2 was studied under the two stimulating sources, IR and blue, available in the Risoe and Daybreak machine. The stimulation was done after the sample was irradiated with 1 Gy of beta dose. The dose source was Strontium (^{90}Sr) which is a radioactive β source. Under IR stimulation the emission was studied using three different filters. They are Schott bg39 of 2 mm thickness, Hoya u340 of 7.5 mm thickness, and Corning 7-59 of 4 mm thickness.

The transmission curves for the above filters are given in figures 29-31. A combination of bg39 and Corning 7-59 filters was also used for IR stimulation. The transmission of this combination is given in figure 31. Theses curves were generated by the 'Filtermultiplier' software (v1.2).

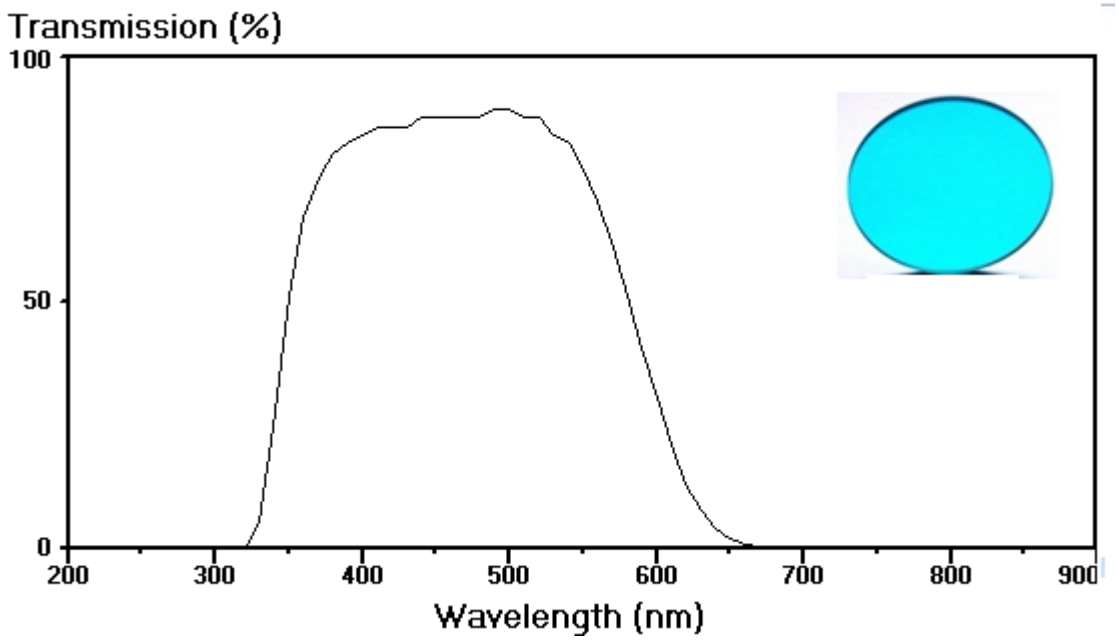

Figure 29. Transmission curve for schott bg39 filter of 2 mm thickness.

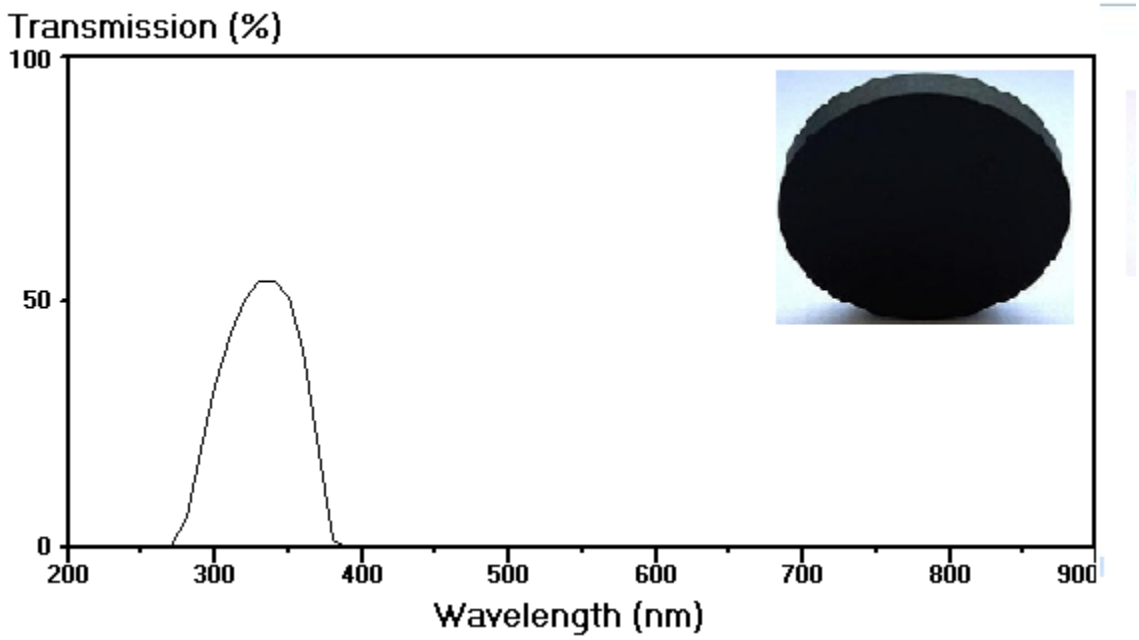

Figure 30. Transmission curve for Hoya u340 filter of 7.5 mm thickness

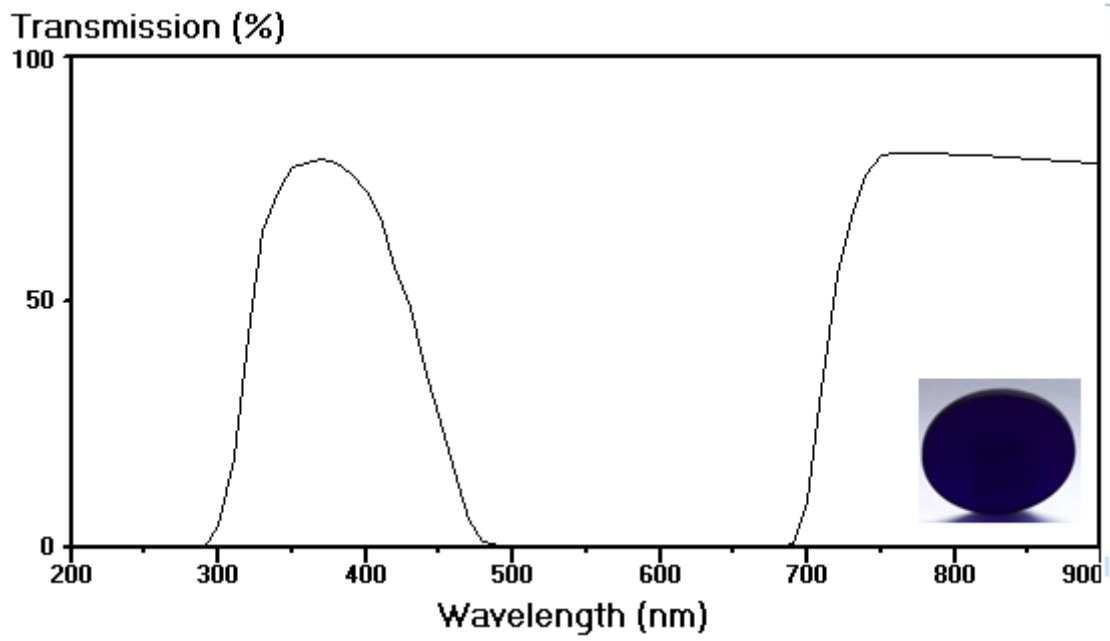

Figure 31. Transmission curve for Corning 7-59 filter of 4 mm thickness.

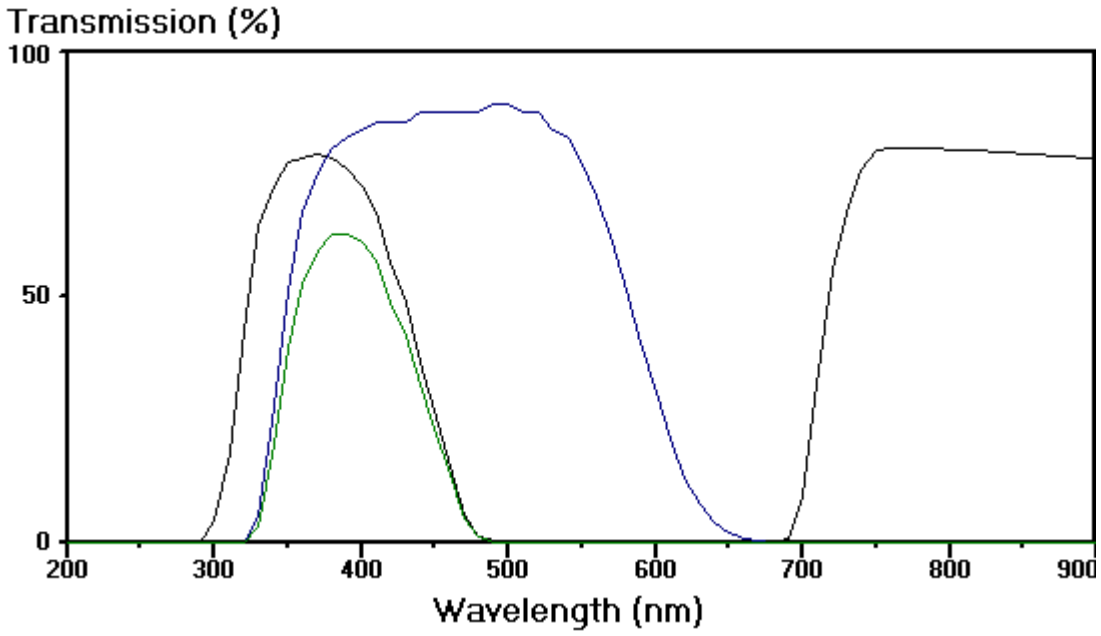

Figure 32. The green curve is the resultant transmission of the bg39 and Corning 7-59 filter. (combination of figure 29 and 31)

5.5.3.1 IR-OSL

For IR-OSL infrared LEDs having emission at 870 nm are used in the Risø TL/OSL luminescence reader. The model used here is TL/OSL-DA-20. The maximum power by the 21 IR LEDs used is approximately 145 mW/cm^2 at the sample position. The decay curve obtained by the IR-OSL using bg39 filter is given in figure 33. Here the maximum count is above 525,000.

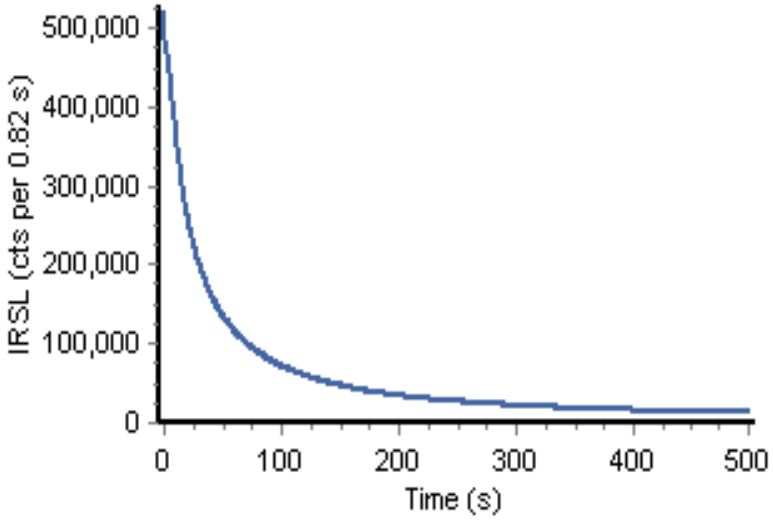

Figure 33. Decay curve for IR OSL with bg39 filter.

The decay curve obtained for IR-OSL with bg39 + 7-59 filter is shown in figure 33. The maximum count here is around 125000.

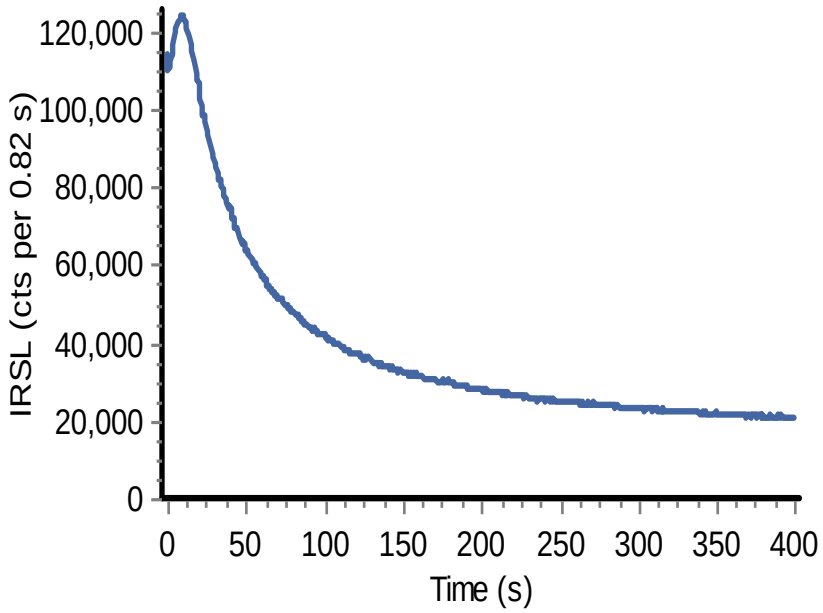

Figure 34. Decay curve for IR-OSL with bg39 +7-59 filter

The decay curve obtained for IR-OSL with u340 filter is shown in figure 34. The maximum count is approximately 325000.

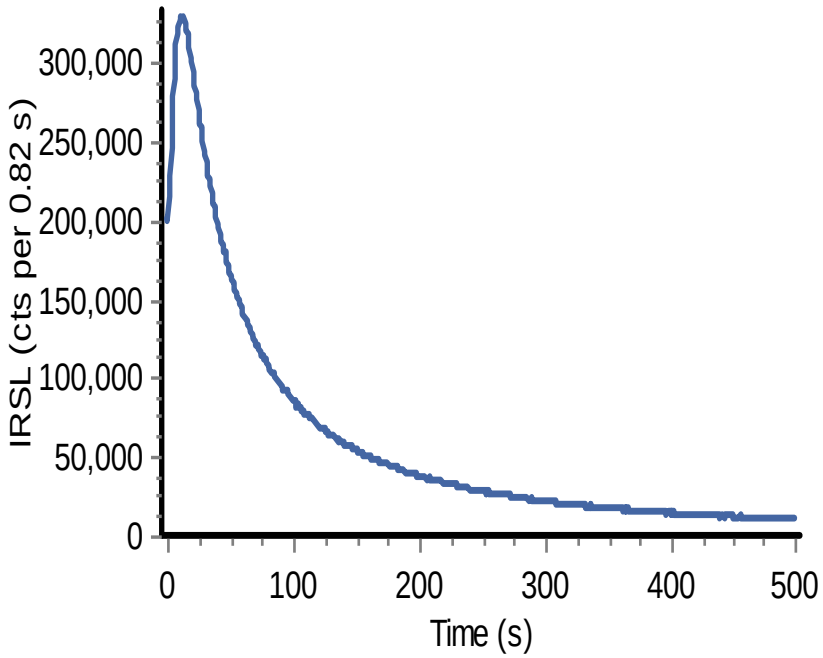

Figure 35. Decay curve for IR-OSL with u340 filter

From the above decay curves shown in figure 33, 34 and 35 it can be seen that for IR stimulation the emission in the 330 to 600 nm range is 4.2 times more than that in the 330 to 480 nm range and 1.6 times more than that in the 280 to 370 nm range. Therefore it can be inferred that the phosphor has maximum emission in the range 480 nm to 600 nm for IR stimulation.

5.5.3.2 Blue OSL

For blue OSL, blue LEDs having emission at 470 nm arranged in four clusters of seven LEDs each is used. The total power by these 28 LEDs is approximately 50 mW/cm^2 at the sample position. A green long pass filter (GG-420) is incorporated in front of each blue LED cluster to minimise the amount of directly scattered blue light from reaching the PMT (Risø manual). The decay curve obtained for blue OSL with uv340 filter is shown in figure 36. The maximum count is approximately 17500000. This is the maximum count compared to the other previous counts; around 33 times more than that obtained for IR stimulation with bg39 filter. Thus the maximum emission is from blue stimulation and is in the range 280 to 370 nm.

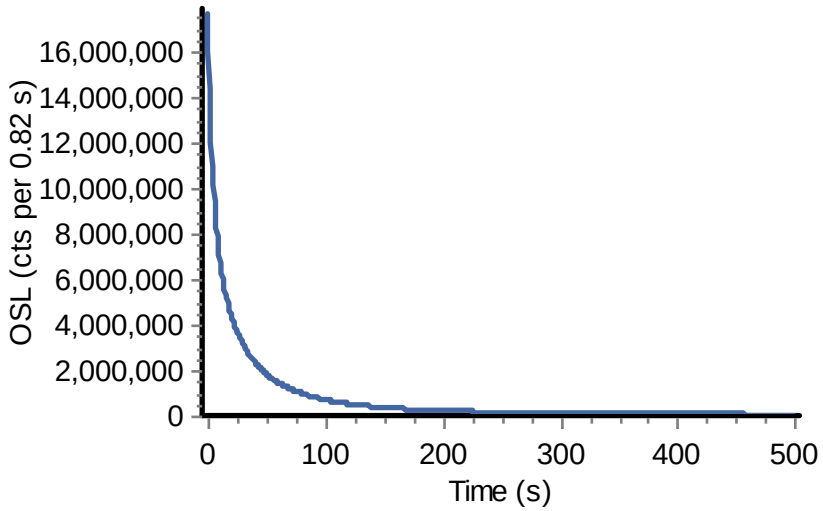

Figure 36. Decay curve for blue OSL with u340 filter

5.5.4 OSL dose response

Figure 37 gives the OSL dose response of this phosphor. It gives a linear dose response till around 100 Gy. After that non-linearity is observed but still an increase in emitted counts is observed with increasing dose. The dose response curve was fitted to the following single saturation exponential.

$$I = I_0\left[1-\exp\left(\frac{-D}{D_0}\right)\right] \quad \text{..... (13)}$$

Where,

I = measured intensity

I_0 = saturated intensity at infinite dose

D = given dose

D_0 = dose where the saturation begins (figure 38). Its intensity is 63% of the saturation intensity

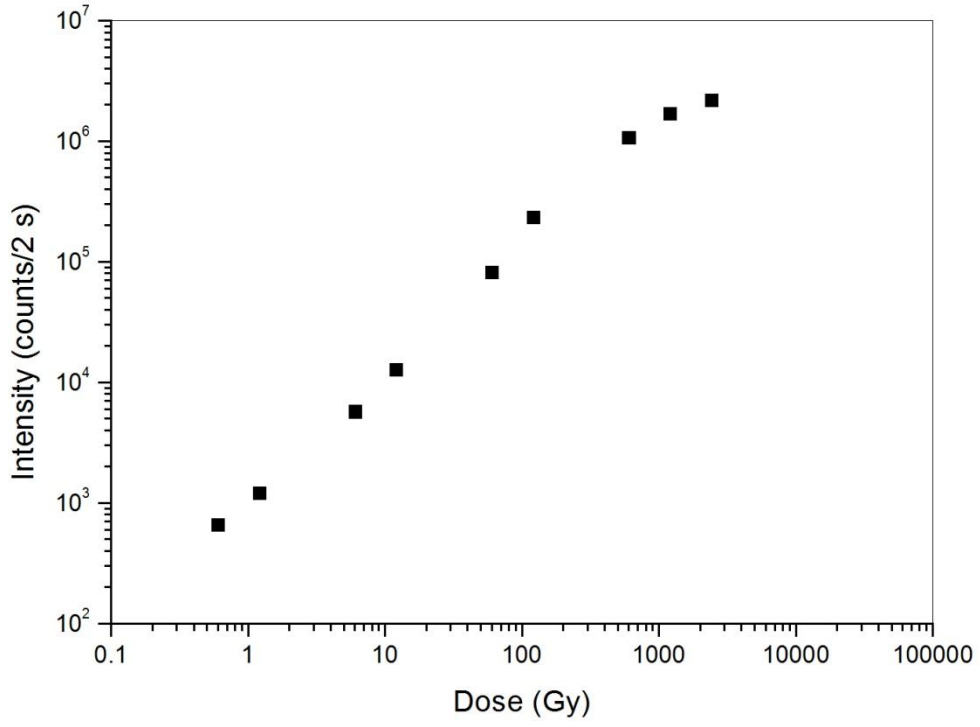

Figure 37. OSL dose response

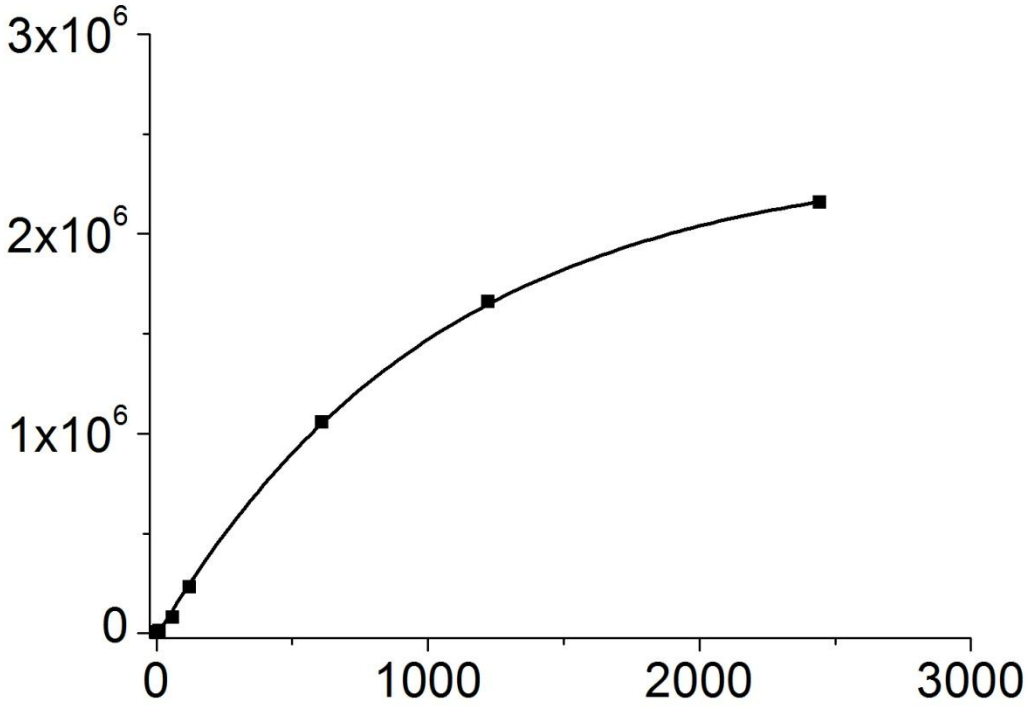

Figure 38. OSL dose response (exponentially fitted)

The graph for the above equation is given in figure 38. The maximum detectable dose is $2D_0$. At this dose the signal intensity is 86% of saturation intensity. The calculated D_0 is 1037 Gy. So the maximum detectable dose ($2D_0$) is 2074 Gy. Figure 38 gives the exponentially fitted dose response curve.

5.6 Correlation between TL and OSL of the synthesised CaF_2

Efforts have been made in the past to study the relation between TL and OSL properties of natural CaF_2 [36, 37]. In the case of the synthesised CaF_2, the correlation between TL glow curve peaks and the OSL decay curve intensity is reported here. Figure 39 shows the glow curve of the phosphor. The glow curve shows three peaks. A peak is found at the low temperature region of around 90 ˚C. This being a very shallow trap is of no use for dosimetric applications. The next peak is around 210 ˚C. This peak is just right for dosimetric applications because it is at a temperature region where dark counts are not so prominent and where the trap depth is not shallow. The third and the last peak is around 490 ˚C. This peak

disappears after a few TL cycles. This destruction of the high temperature peak has also been reported by Romero [38].

An OSL done without doing a prior TL would contain all the TL luminescence causing trapped electrons. In order to find the correlation between the TL luminescence and the OSL luminescence, a TL is done on the sample till the first peak is removed. Then the OSL is measured. This OSL measurement is compared with the OSL which measured without any prior TL. The difference between the two OSL measurements gives the contribution of the first peak to the OSL. Similarly it is done for the second and the third peak.

This was done as follows: First the sample was subjected to a blue OSL cycle (figure 40). Then TL was done till 130 ˚C to remove the first peak (figure 41). Again the OSL cycle was repeated (figure 42) which was followed by TL till 400 ˚C (figure 43) to remove the second peak. The glow curve of this TL shows that the peak is shifted to the lower temperature region after the OSL. The OSL done after this TL showed no luminescence other than the constant background (figure 44)

In the initial OSL cycle the maximum count in the shine down curve was 1,200,000. This count dropped to 850,000 after the first peak was removed by the TL done till 130 ˚C. It reduced to the background noise after the second peak was removed by the TL done till 400 ˚C. This shows that the first peak contributed around 30% to the total luminescence in the OSL decay curve. The remaining 70% of the luminescence was due to the second peak. The third high temperature peak which was unstable does not seem to have any effect on the OSL, or it might be destroyed after the first OSL cycle.

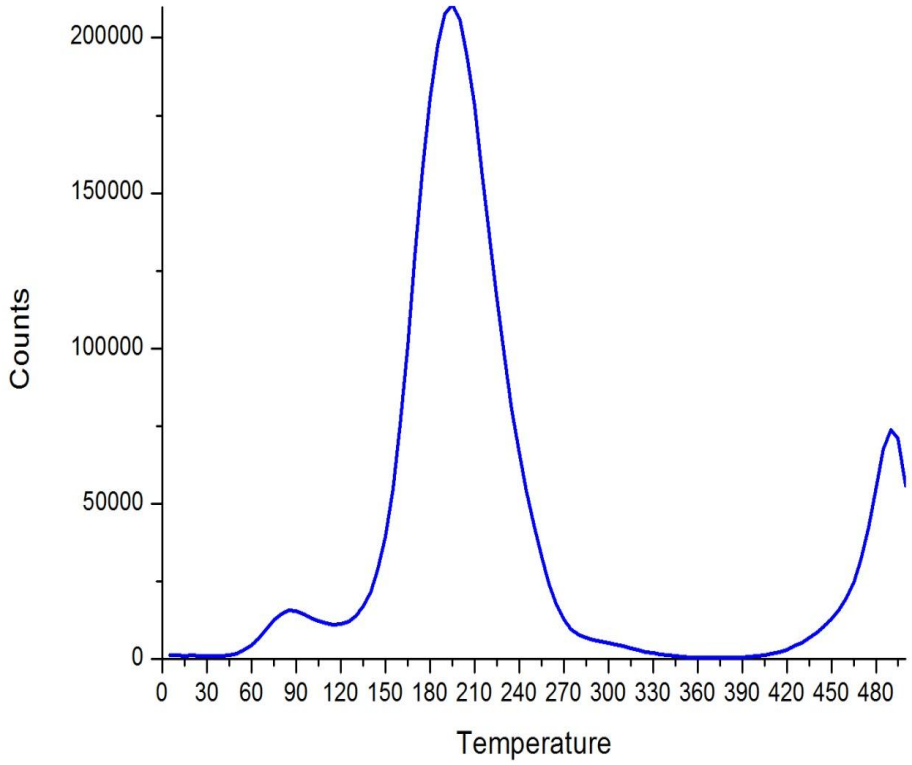

Figure 39. Glow-curve of CaF_2

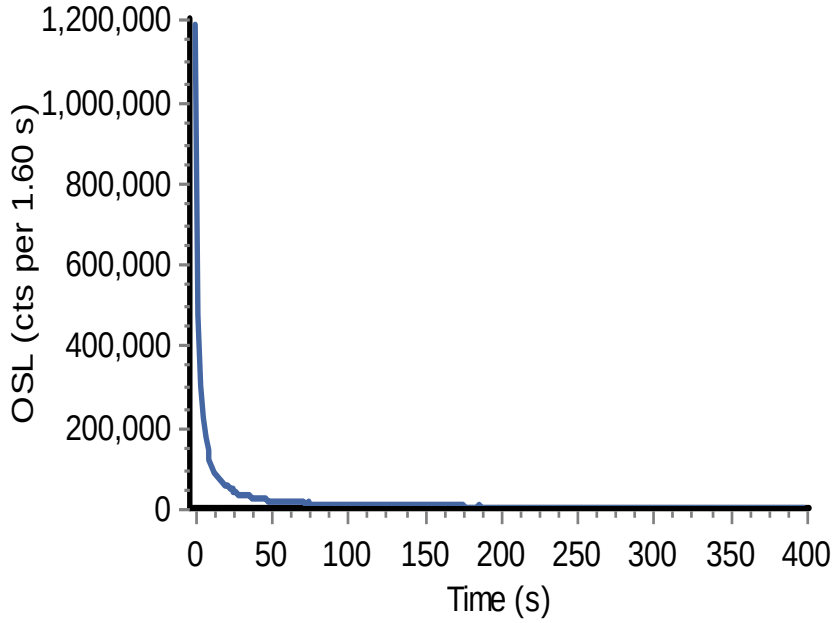

Figure 40. OSL decay curve without any prior TL

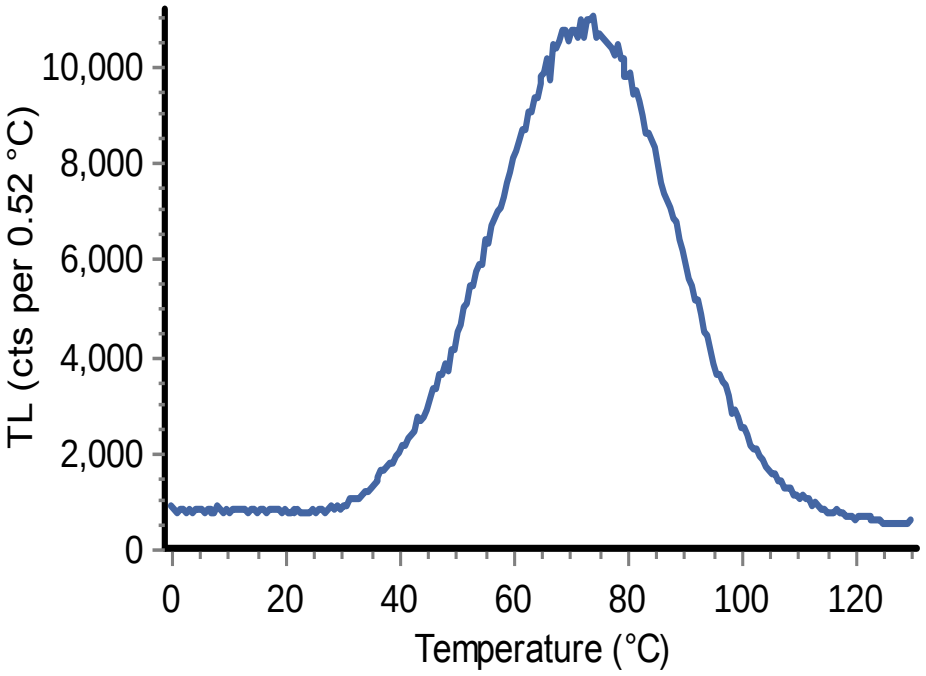

Figure 41. TL till 120 ˚C to remove the first peak

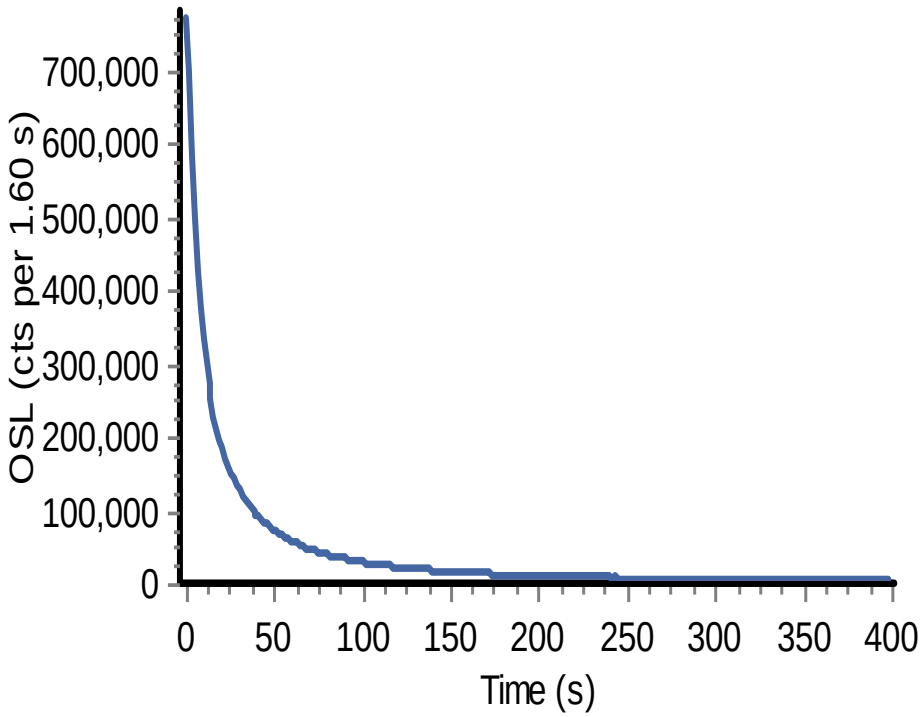

Figure 42. OSL decay curve after the first peak was thermally removed

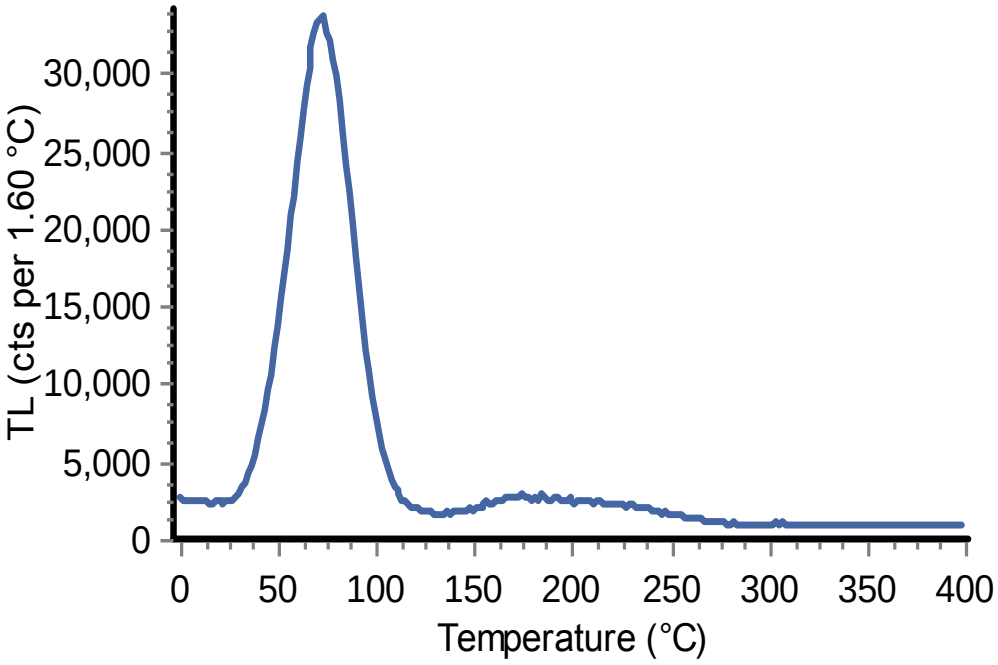

Figure 43. TL till 400 ˚C to remove the second peak.

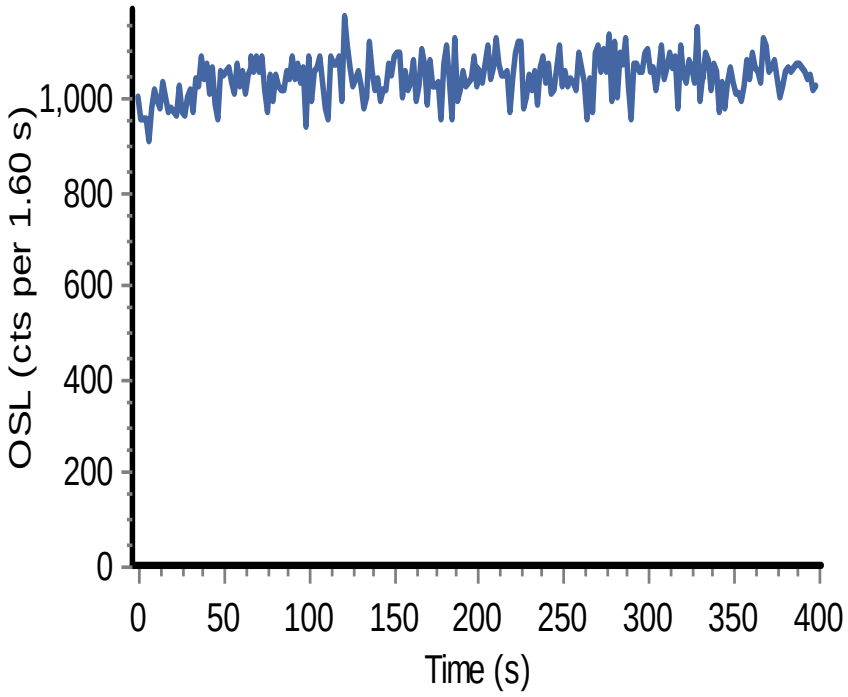

Figure 44. OSL decay curve after all the peaks are removed. It shows only the constant background counts

5.7 OSL vs TL debate

OSL does offer many advantages over TL. The changes in the properties of some of the sample due to heating during TL do not happen in OSL. Repeated measurements can be made in OSL if the stimulating light is not of high enough intensity to deplete all the trapped charges. Repeated measurements can also be made if pulsed OSL is used. In the case of TL this is not possible because once the TL measurement is made the signal is totally erased. OSL does not require the high temperatures needed in the case of TL. This implies lesser power consumption. This is especially beneficial for space based dosimetry.

There are certain traps that are so deep that they cannot be affected by the normal TL measurements. Such traps can be accessed using OSL of suitable wavelength. The problem of thermal quenching where the recombination takes place non-radiativly at higher temperature does not occur in the case of OSL which is normally performed at room temperature or at elevated temperatures not high enough for thermal quenching to occur.

The problem of black body radiation does not occur in OSL due to absence of heating. Though some OSL measurements are preformed at elevated temperature those temperatures do not significantly contribute to black body radiation.

5.8 Radioluminescence (RL)

In RL, the sample is kept under irradiation which causes electrons to be trapped in the optically sensitive electron trap. The constant irradiation causes electrons to move from valence band to conduction band from where they may recombine or be trapped emitting luminescence which is a property of the trap [39]. This phenomenon was first investigated by Trautmann *et al* [39]. They pioneered a new method of luminescence dating based on radioluminescence measurements of potassium feldspar. Also new insights about the distribution and kinetics of trapped charges can be obtained by Radioluminescence measurements. Proper instrumentation has also been developed in order to study RL [40-42].

The luminescence emission in IR region caused by the radiative trapping of electrons stimulated by ionizing radiation is called infrared radioluminescence (IRRL). The synthesised CaF_2 was tested for IRRL. To accomplish this an automated Risø TL/OSL-DA 20 reader with a RL attachment described by Lapp *et. al.* and Buylaert *et al.* [41,42] is used. A $^{90}Sr/^{90}Y$ β

source was used for irradiation. It has a dose rate of 0.055 Gy/s. For photon detection a Hamamatsu H7421-50 photomultiplier tube was used. It has a spectral response in the region 380-890 nm. Chroma D 900/100 interference filter with a band pass transmission at 850-945 nm was used. The net transmission of filter and the photomultiplier tube was in the region 855 ± 27 nm. Bleaching of the sample prior to the irradiation was done with UV LEDs of 1 W optical power. The emission of this UV LEDs is at 395 nm with 700 mW/cm^2 irradiance on the sample position. The result of this measurement was that CaF_2 does not give IRRL.

5.9 Conclusion

The as prepared phosphor was found be TL insensitive. Annealing treatment was done on it to improve its TL characteristics. The best annealing parameters were found by the systematic experimentations using the various combinations of temperature, duration and atmosphere. It is found that annealing temperature of 600 ˚C is the best annealing temperature when the annealing duration is kept constant at 1.5 h. However, when annealing durations were varied keeping the annealing temperature constant at 500 ˚C and 600 ˚C, it was found that the former gave better results. Thus it was concluded from the observations that the phosphor annealed at 500 ˚C for 2.5 h become maximum luminescent.

The above results indicates that as the annealing parameters are varied systematically, the luminescence properties are enhanced up to a certain extent, beyond this if the annealing parameters, i.e. temperature or duration, are increased there is a reversal in the observed trend. The decrease in the crytallinity beyond this point and the increase in the crytallinity till this point of reversal could be the reason for the observed trend in the luminescence of the material [9, 10].

Regarding its TL characteristics it is found to follow the general order kinetics. This is in accordance with what is reported in literature [43]. The value of b, calculated by the glow-curve shape method and using Chen's graph [18] is 2.3. The activation energy *E* of this phosphor was found by various methods. By the initial rise method *E* was found to be 1.04 eV. Using the variable heating rate method *E* was found to be 1.00 eV. From the peak temperature value, *E* was calculated using Randall and Wilkins' formula [13] given in equation 9 and by Urbach's [22] formula given in equation 10. Randall and Wilkins' formula gave the value of *E* as 1.00 eV and Urbach's formula gave the value of *E* to be 0.93 eV. In

the glow curve shape method three values of E was calculated using the value of τ, δ, and ω in equation 7. E was found to be 1.08 eV, 1.01 eV, and 1.04 eV for the values τ, δ, and ω respectively. The symmetry factor μ, of the glow curve is 0.54. The minimum detectable dose is 5 mGy and it reaches saturation around 2 kGy. These values depend not only on the phosphor composition but also in the synthesis method and annealing conditions. This explains the lack of agreement among different authors. Different synthesis technique could cause major variations in the glow curve [44]. Due to this the synthesised nano size Calcium Fluoride has not been compared with bulk sized Calcium Fluoride. Natural Calcium Fluoride from different origins also has been reported to have different glow curve shape [2, 3, 7].

From the above TL characteristics it can be concluded that this phosphor has sufficient activation energy of around 1.04 eV and a long dynamic range of 5 mGy to 2 kGy, to make it suitable for dosimetric applications. This phosphor is especially suitable for environmental dosimetry due to its high sensitivity. Lack of tissue equivalence prevents its use for medical dosimetry.

Regarding its OSL characteristics it is seen from the decay curves in figure 32, 33 and 34 that for IR stimulation the emission in the 330 to 600 nm range is 4.2 times more than that in the 330 to 480 nm range and 1.6 times more than that in the 280 to 370 nm range. Thus from the above it can be inferred that the phosphor has maximum emission in the range 480 to 600 nm for IR stimulation. Blue stimulation with detection in the UV region (280 to 370 nm) gave the maximum count which was around 33 times more than that obtained for IR stimulation in the 330 to 600 nm range. This emission spectra gives indications about the distribution of recombination centres in the phosphors since the emission spectra is dependent on the recombination centre and not on the trapping centres. Greater intensity of the emission in a particular wavelength band indicates higher concentration of recombination centres in the corresponding area.

This phosphor gave a linear dose response till around 100 Gy. After that non-linearity is observed but still an increase in emitted counts is observed with increasing dose. The phosphor response saturates around 2500 Gy.

In the study to find the correlation between the TL and blue OSL of the phosphor, it was found that the first peak in the TL glow curve contributed around 30% to the total luminescence in the OSL decay curve. The remaining 70% of the luminescence was due to the second peak. The third high temperature peak which was unstable does not seem to have

any effect on the OSL, or it might be destroyed after the first OSL cycle. This indicates that most of the thermal traps and the optical traps may be the same for this phosphor.

The phosphor did not give any response for IRRL. This implies that the electron density at the corresponding trap is zero. It is probable that there are no traps at the corresponding level i.e. at the level where its trapping will give emission in the IR region.

References

[1]. Keck, B. D., Guimon, R. K., and Sears, D. W. G., (1986). Chemical and physical studies of type 3 chondrites, VII. Annealing studies of the Dhajala H3.8 chondrite and the thermal history of chondrules and chondrites. *Earth Planet sc let.* 77, pp. 419.

[2]. El-Kolaly, M. A., Rao, S. M. D., Nambi, K. S. V. and Ganguly, A. K., (1980) Observations on a high temperature peak in the thermoluminescence of fluorites, *Pramana,* 14 (2), pp. 165,

[3]. Sunta, C. M., (1984). A Review of Thermoluminescence of Calcium Fluoride, Calcium Sulphate and Calcium Carbonate. *Radiat. Prot. Dosim.* 8 (1-2), pp. 25.

[4]. Sunta, C. M., (1985). Thermoluminescence of calcium-based phosphors. *Nucl. Tracks.* 10 (½), pp. 47.

[5]. Sunta, C. M., Yoshimura, E. M., and Okuno, E., (1994). Sensitization and supralinearity of CaF_2: natural thermoluminescent phosphor. *phys.stat.sol. (a)* 142, pp. 253.

[6]. Nedelcu, M., Podina, C., Jipa, S., Setnescu, R., Setnescu, T., Gorghiu, L. M., Dumitrescu, C., Popescu, I. V., Oros, C., Zaharescu, T. *et al* (2010). Dosimetric features of natural fluorite from Romania. *Journal of science and arts* 10, pp. 287.

[7]. Sohrabi, M., Abbasisiar, F., and Jafarizadeh, M., (1999). Dosimetric Characteristics of Natural Calcium Fluoride of Iran. *Radiat Prot Dosim.* 84 (1-4), pp. 277.

[8]. Bortolot, V. J., (2000). A new modular high capacity OSL reader system. *Radiat. Meas.* 32, pp. 751.

[9]. Biswas, R. H., and Singhvi, A. K., (2013). Anomalous fading and crystalline structure: studies on individual chondrules from the same parent body. *Geochronometria* 40(4), pp. 250.

[10]. Sears, D. W. G., (1988). Thermoluminescence of meteorites: Shedding light on the cosmos. *Int J Rad Appl Instrum D* 14 (1-2), pp. 5.

[11]. Li, S. H., and Hsu, P. C., (1990). The role of annealing: effect on CaSO4:Dy phosphor with manganese and sodium impurities. *Radiat. Prot. Dosim.* 33 (1/4), pp. 147.

[12]. Chougaonkar, M. P., Kumar M., and Bhatt, B. C., (2012). Testing of Phosphors for their use in Radiation Dosimetry: Detailed Procedure and Protocol. *International Journal of Luminescence and Applications* 2 (Special Issue: III), pp. 194.

[13]. Randall, J. T., and Wilkins, M. H. F., (1945). Phosphorescence and electron traps. I. The study of trap distributions. *Proceedings of Royal Society of London* 184, pp. 366.

[14]. Garlick, G. F. J., and Gibson, A. F. (1948). The electron trap mechanism of luminescence in sulphide and silicate phosphors. *Proceedings of Physics society* 60, pp. 574.

[15]. Partridge, J. A., and May, C. E., (1965), *J. chem. Phys.,* 42, pp. 797.

[16]. Muntoni, C., Rucci, A., and Serpi, A., (1968), *Ricevca Sci.,* 38, pp. 162.

[17]. Capelletti, R., and de Benedetti, E., (1968), *Phys. Rev.,* 165, pp. 981.

[18]. Chen, R., (1969), *J. Electrochem. Soc.*, 116, pp. 12547.

[19]. Taylor, A., (1970), *Phys. Stat. Sol.,* 37, pp. 401.

[20]. Shenker, D., and Chen, R., (1971). Numerical curve fitting of general order kinetics glow peaks, *J. Phys. D: Appl. Phys.,* 4, pp. 287.

[21]. Pagonis, V., Kitis, G., and Furetta, C., (2006). *Numerical and Practical Exercises in Thermoluminescence,* New York: Science and Business Media, Inc..

[22]. Urbach, F., (1930). *Winer Ber. IIa* 139**,** pp. 363.

[23]. Bohum, A., (1954). *Czech. J. Phys.* 4 pp. 91.

[24]. Porfianovitch, I.A., (1954). *J. Exp. Theor. Phys. SSSR,* 26, pp. 696.

[25]. Booth, A.H., (1954). *Canad. J. Chem.* 32, pp. 214.

[26]. Chen, R., and Winer S.A.A., (1970). *J. Appl. Phys.* 41, pp. 5227

[27]. Merz, J. L., and Pershan, P. S. (1967) Charge conversion of irradiated rare-earth ions in calcium fluoride. *Phys. Rev.* 162, pp. 217-247.

[28]. Sunta, C. M. (1985) Thermoluminescence of calcium-based phosphors. *Nucl. Tracks.* 10 (1/2), pp. 47-53

[29]. Bulur, E., Bøtter-Jensen, L., Murray, A. S., (2001). LM-OSL signals from some insulators: an analysis of the dependency of the detrapping probability on stimulation light intensity. *Radiation Measurements,* 33, pp. 5.

[30]. Markey B.G., Bøtter-Jensen L., Poolton N.R.J., Christiansen H.E., and Willumsen F., (1996). A new sensitive system for measurement of thermally and optically stimulated luminescence. *Radiat. prot. Dosim.* 66 (1/4), pp. 413.

[31]. McKeever S.W.S., Markey B.G. and Akselrod M.S. (1996a) Pulsed optically stimulated luminescence dosimetry using α-Al2O3:C. *Radiat. Prot. Dosim.* 65, pp. 267

[32]. Bos, A. J. J., and Wallinga. J., (2009). Optically stimulated luminescence signals under various stimulation modes assuming first-order kinetics. *Phys. Rev. B.* 79, pp. 195118.

[33]. Biernacka, M., and Mandowski, A., (2013). Investigation of regeneration effect of blue luminescence in NaCl using variable delay optically stimulated luminescence (VD-OSL), *Radiation Measurements.* 56, pp. 31.

[34]. McKeever, S.W.S., Moscovitch, M., and Townsend, P.D., (1995). *Thermoluminescence Dosimetry Materials: Properties and Uses.* Nuclear Technology Publishing,

[35]. Calderon, T., Millan, A., Jaque, F., Sole, G. J., (1990). *Nucl. Tracks Radiat. Meas.* 17 (4), pp. 557.

[36]. Polymeris, G. S., Kitis, G., Tsirliganis, N. C., (2006).A Correlation between TL and OSL properties of CaF2:N. *Nuclear Instruments and Methods in Physics Research B* 251 pp. 133.

[37]. Chougaonkar, M.P., and Bhat, B. C., (2004). Blue light stimulated luminescence in calcium fluoride, its characteristics and implications in radiation dosimetry. *Radiation Protection Dosimetry.* 112 (2), pp. 311.

[38]. Romero, H., (1995) Calcium Fluoride, Department of Physics, University of Cincinnati, Cincinnati, Ohio.

[39]. Trautmann T., Krbetschek M. R., Dietrich A., and Stolz W., (1999). Feldspar radioluminescence: a new dating method and its physical background. *J. Lum.* 85, pp. 45.

[40]. Erfurt, G., Krbetschek, M.R., Bortolot, V.J., Preusser, F., (2003). A fully automated multi-spectral radioluminescence reading system for geochronometry and dosimetry. *Nuclear Instruments and Methods in Physics Research Section B: Beam Interactions with Materials and Atoms,* 207 (4), pp. 487.

[41]. Buylaert, J-P., Jain, M., Murray, A. S., Thomsen, K. J., and Lapp, T. (2012). IR-RF dating of sand-sized K-feldspar extracts: A test of accuracy. *Radiation Measurements, 47* (9), pp. 759.

[42]. Lapp, T., Jain, M., Thomsen, K. J., Murray, A. S., and Buylaert, J-P., (2012). New luminescence measurement facilities in retrospective dosimetry. *Radiation Measurements, 47* (9), pp. 803.

[43]. Ogundare, F.O., Balogun, F. A., and Hussian, L. A., (2004). Kinetic characterization of the thermoluminescence of natural fluoride, *Radiation Measurements, 38*, pp. 281.

[44]. Kerikmae, M.,(2004) Some luminescent materials for dosimetric applications and physical research, *PhD thesis, University of Tartu, Estonia.*